1968

Corrosion rates and electrokinetics of cobalt and cobalt-rich cobalt-iron alloys in sulfuric and hydrochloric acids

Cheng Tzong Horng

Department:

77p.

CORROSION RATES AND ELECTROKINECTICS OF COBALT AND COBALT-RICH COBALT-IRON ALLOYS IN SULFURIC AND HYDROCHLORIC ACIDS

BY

CHENG TZONG HORNG, 1940

A

THESIS

submitted to the faculty of

THE UNIVERSITY OF MISSOURI-ROLLA

in partial fulfillment of the work required for the

Degree of

MASTER OF SCIENCE IN METALLURGICAL ENGINEERING

Rolla, Missouri

1968

Approved by

M. E. Straumanis (Advisor) W. J. James

H. R. Leighly, Jr.

ABSTRACT

Corrosion rates for Co and Co-rich Co-Fe alloys were determined in sulfuric and hydrochloric acids under both deaerated and oxygenated conditions. For the purpose of comparison, corrosion rates of Co cut from metal sheet were also determined in the same environments as those of sintered alloys. Sintered alloys were inferior to solid Co as corrosion resistant materials. It was found that the surface was more corrosion resistant than the interior. Thus after long exposure to the corrosive acid, the samples became porous inside while the surfaces remained substantially intact.

Oxygen had a pronounced effect in accelerating the corrosion of Co and Co-rich alloys, although it is known to have little effect on the corrosion of Fe in acids.

The activation energy of dissolution of Co was determined by measuring the maximum corrosion rate in H_2SO_4 at four temperatures. The results showed that the energy barrier for the dissolution of Co in deaerated acid is about twice as large as in aerated acid.

Corrosion potentials of the alloys were measured in both HCl and H_2SO_4 solutions. Co and Co-Fe alloys, respectively, showed a more active corrosion potential in HCl than in H_2SO_4 solutions. However, the corrosion rate studies revealed that Co and Co-Fe alloys were less corrosion resistant in H_2SO_4 than in HCl.

Corrosion rates of Co-Fe alloys were also measured by using cathodic polarization curves. The corrosion rates obtained by

the electrochemical method were throughout a little higher than the rates determined by the weight loss method.

Anodic polarization and passivation behavior of Co-Fe alloys were studied in H_2SO_4 and HCl solutions. The reason why the Co anode achieved passivity in H_2SO_4 solutions but not in HCl solutions is discussed as due to the formation of a protective film.

ACKNOWLEDGEMENTS

The author would like to express his sincerest thanks to Dr. M. E. Straumanis, Professor of Metallurgy and Research Professor of Materials, for his constant direction and invaluable consultation throughout the course of this investigation.

He would also like to express his thanks to Dr. W. J. James, Professor of Chemistry and Director of the Graduate Center for Material Research, for his continued interest.

The author is grateful for the financial aid received from the Office of Naval Research and the Corrosion Research Council.

TABLE OF CONTENTS

LIST OF FIGURES

FIGURE PAGE

LIST OF TABLES

I. INTRODUCTION

Prior to 1914, cobalt was marketed as cobalt oxide: virtually no cobalt metal was produced. Some experiments were made with this metal, e.g. Haynes prepared cobalt chromium alloys as early as 1842, and it was found that these alloys, named Stellites, were corrosion resistant. R. Bottger[A] was probably the first to show in 1842 that cobalt can be electroplated on other metals. In 1874, G. W. Beardslee[B] received a U.S. patent on electroplating. He claimed that cobalt forms a useful coating which is tenacious, compact, adherent, flexible, and of sufficient thickness to protect metals from corrosion. Watt[C] in 1913, expressed the opinion that the only obstacle to the general use of cobalt for plating instead of nickel was its high price. The cobalt produced at that time was not very pure as it contained nickel, iron, etc. Only in 1956 did the U.S. Bureau of Mines[D] (Rolla branch) announce for the first time production of 99.99% pure cobalt. The world production of cobalt had then reached nearly 14,000 short tons per year.

Pure cobalt has found little practical use, but cobalt-base alloys and many alloys with cobalt additions are used considerably in industry. The use of cobalt as a base together with iron, chromium...or the addition of cobalt to iron alloys is to obtain maximum hot strength and resistance to corrosion. Cobalt is the base material in making permanent magnets.

Despite the present importance of cobalt, relatively little is known about its corrosion resistance.

Observations given in the literature regarding the corrosion resistance of cobalt are often contradictory. The rate at which a

metal corrodes in a solution is dependent on many factors; mainly upon its purity and the concentration and nature of the corrosive agent. As soon as high purity cobalt was available, systematic studies were possible on its behavior in various acids. The information obtained could be useful in determining the corrosion mechanism of cobalt in acids.

The purpose of the present investigation was, therefore, to furnish new data concerning the corrosion rate of pure cobalt in strong acids and the effect on rate of iron additions to the cobalt. It was assumed that this goal could be achieved by:

1. measuring the corrosion rate of pure cobalt and cobalt-rich iron alloys in various aqueous concentrations of H_2SO_4 and HCl in and without the presence of air (oxygen);

2. determining the activation energy of dissolution of pure cobalt in oxygenated and deaerated acid;

3. measuring the hydrogen overvoltage and checking the previous determined corrosion rates by the use of cathodic polarization curves;

4. determine the corrosion potentials of pure cobalt (solid and sintered), and Co-Fe alloys and the critical passivation current density of the same alloys in acids.

II. REVIEW OF LITERATURE

In general, the chemical properties of Co are much closer to those of Ni than to Fe. Co dissolves in aqueous solutions always as divalent ions, Co^{++}, because the cobaltic ion, Co^{+++}, is such a powerful oxidizer that it cannot exist in an aqueous medium. The metal in the solid form is not attacked by water and air below approximately 300°C; above this temperature it oxidizes. The reversible potential of Co, E_o, is -0.277 volt. The metal is, therefore, more active than Ni (E_o = -0.250) but is more noble than Fe (E_o = -0.440). This sequence is also maintained in many irreversible corrosion systems.[1]

The potential-pH equilibrium diagram of the system Co-H_2O at 25°C was established by Deltombe and Pourbaix.[2]

According to Antropov[3] Co belongs to the group of cathodic materials on which the rate of hydrogen evolution is limited by the rate of the recombination of hydrogen atoms.

Data obtained by Young[4,5] show that the corrosion resistance of Co in dilute sulfuric acid, acetic acid and ammonia solutions is of the same order as that of nickel. Co is more resistive to air-free 5% sulfuric acid than is Fe. Air increases the rate of corrosion significantly. Co and Ni display about the same resistance to aerated 1N-HCl.

Hedges[6] reported that Co is vigorously attacked by concentrated HNO_3 at room temperature but becomes passive at about -11°C. Hedges[7] also determined the anodic and passivation behavior of Co in various other solutions. His results showed that Co may be active or passive as an anode, depending on the nature and

concentration of the electrolyte. Co can be passivated by an anodic current at a lower current density than Fe in all concentrations of H_2SO_4. In solutions of hydrochloric acid, nitric acid, ammonia sulfate and sodium sulfate, Co does not become passive in the concentration range studied.

Heusler[8] investigated the kinetics of passivation and activation of Co in o-phosphoric and perchloric acid solutions. He found that Co becomes passive after being covered with at least one complete monolayer of adsorbed hydroxyl groups. In the stationary state the layer seems to be composed of more than one oxide phase. The higher oxide dissolves very slowly, while the lower oxide dissolves rapidly. Furthermore, he concluded from his experimental results that the kinetics of deposition and dissolution of Co, Fe, and Ni follows the same rules, and, hence, is based on the same reaction mechanism and a similar electrochemical behavior.

Bond's investigation of Fe-Co alloys[9] corroding in 1N-H_2SO_4 showed that corrosion rates of Fe-rich alloys are higher in deaerated than in aerated solutions, while corrosion rates of Co-rich alloys are much less in deaerated than in aerated solution. His corrosion potential measurements showed that increasing Co content renders the Fe-Co alloy more noble. The cathodic polarization curves of Fe-Co alloys in hydrogen saturated 1N-HCl at 25°C exhibit Tafel behavior over a considerable current density range.

The equilibrium phase diagram of Co-rich Co-Fe system is shown in Fig. 1.[10] The main feature of the equilibrium diagram is the extremely narrow solidification range. At 600°C, the two-phase region between the body-centered cubic solid solution and the

face-center cubic cobalt-rich solution extends from 75 to 85.5 at. % Co. At lower temperatures it is probable that the solid solubility of iron in cobalt is approximately 10 at. %. Iron depresses the temperatures of both the magnetic and polymorphic transformations ($\varepsilon' \rightleftharpoons \alpha$) in cobalt.

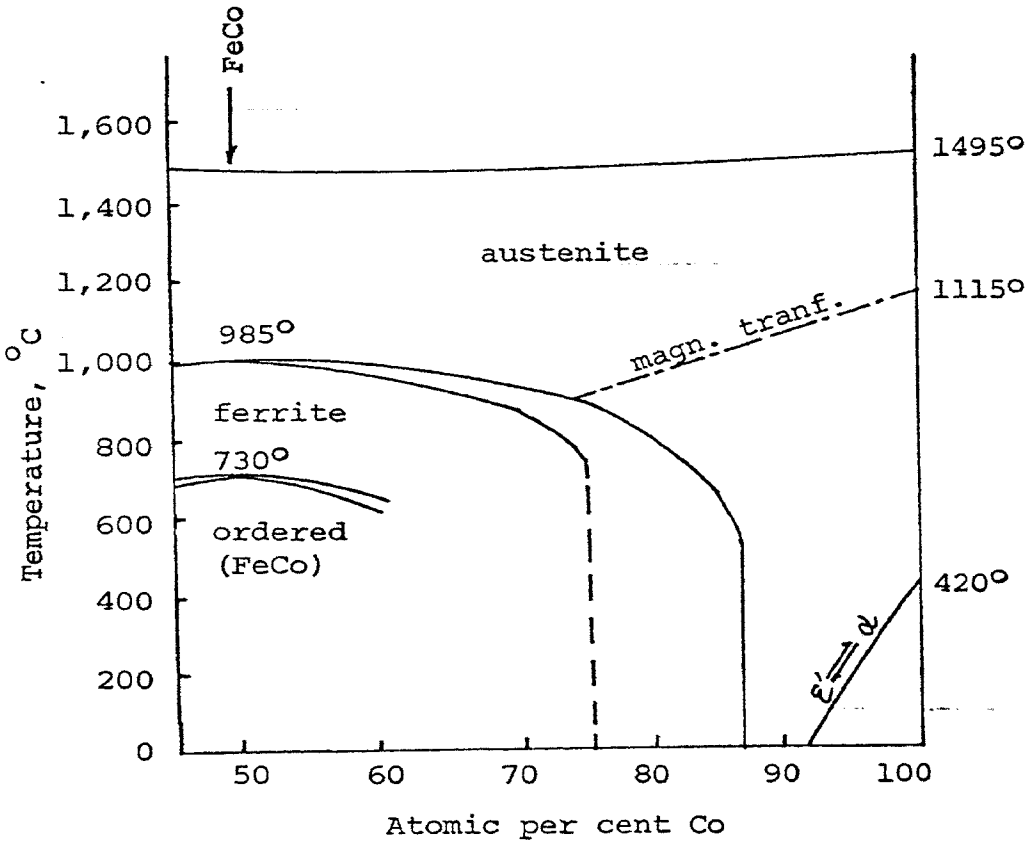

Fig. 1. The Co-rich Co-Fe equilibrium diagram

III. EXPERIMENTAL

A. Materials Used in this Investigation

The corrosion rate of a metal in an acid solution depends on many factors. The purity of the metal and of the acid are most important. It is, therefore, essential to know the purity of metals and of the acid used for corrosion rate determinations.

Most of the Co-Fe alloys of the present investigation were made by the powder metallurgy method. High purity electrolytic powders of fine particle size (-200 mesh) from Fisher Scientific Co. were used.

The composition of the Co powder, according to the label on the container was as follows in wt. %.

Ni	0.05
Cu	0.001
Fe	0.001
S	0.0134
C	0.027

The Fe powder contained in wt. %:

Fe^{++}	93.6
Ni	0.003
S	0.02

0.4% of the powder was insoluble in H_2SO_4.

The Co sheet used for comparison was obtained from Sherritt Gordon Mines Inc., Alberta, Canada, and has a composition according to the manufacturer (in wt. %):

Co	99.9
Ni	0.1
Cu	0.008
Fe	0.05

The acids were of reagent grade and conformed to ACS specifications. A definite concentration of the acid was prepared from the reagent by dilution with distilled water and the normality was checked by titration.

B. Sample Preparation

Most of the Co-Fe alloys were prepared by the powder metallurgy method. Calculated amounts of Co and Fe powders were carefully weighed on an analytical balance, and then mixed in a mortar. The mixtures were spread in a thin layer on the bottom of porcelain boats and pushed into an alumina tube, which was inserted into a horizontal furnace. After flushing the tube with high purity hydrogen for 30 minutes the furnace temperature was increased to 800°C with hydrogen circulation continuing. At this temperature, the oxides were reduced to metals.[11] After four hours in hydrogen at 800°C, the alumina tube was removed from the furnace and air cooled to room temperature.

Two grams of the freshly reduced powders were poured into a round steel die and were compressed at 160,000 psi. Then the plates were sintered in a vertical Metal Research High Temperature Laboratory Furnace and kept for eight hours in a hydrogen atmosphere at 100°C less than the melting point of the respective alloys. The final sintered products, cooled in the furnace to

room temperature, had the dimensions of about 14 mm in diameter and were about 3 mm thick; they looked like solid metal plates.

The corrosion rate measurements were conducted according to ASTM recommendations.[12] To minimize the experimental error in corrosion rate measurements, at least two specimens were used for each measurement. If the results in two specimens did not deviate more than 25% from each other, the average value was taken. If the results deviated more, the measurements were repeated.

For the weight loss method, a small hole was first drilled near the periphery of the plate. The surface of the samples was then smoothed with metallographic emery paper. After washing with distilled water and acetone, the samples were annealed in hydrogen at 700°C to relieve the mechanical stress due to drilling and polishing. The annealed samples were weighed on an analytical balance, and carefully measured with a micrometer. The samples were pickled in 4N HCl just before immersion into the acid in order to more rapidly approach the steady corrosion rate and to improve the reproducability.

The electrodes for potential measurements were made as follows: the samples were mounted in lucite using a metallographic mounting press as shown in Fig. 2; the glass tubing was sealed in with rubber cement and electrical contacts were established by means of mercury drops. The electrodes were polished immediately before each run.

C. Apparatus

The apparatus, Fig. 3, used for the corrosion rate measurements consisted of a 250 ml wide-mouth flask with a tightly fitting

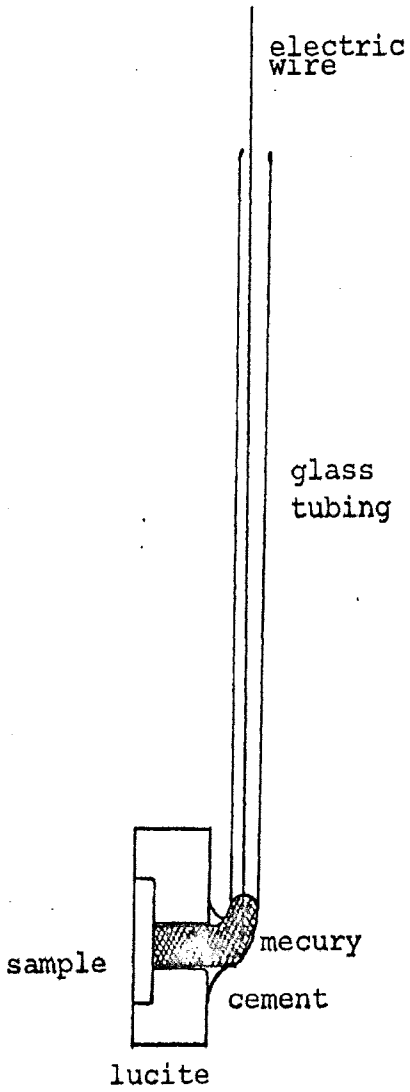

Fig. 2. Electrode for potential measurement

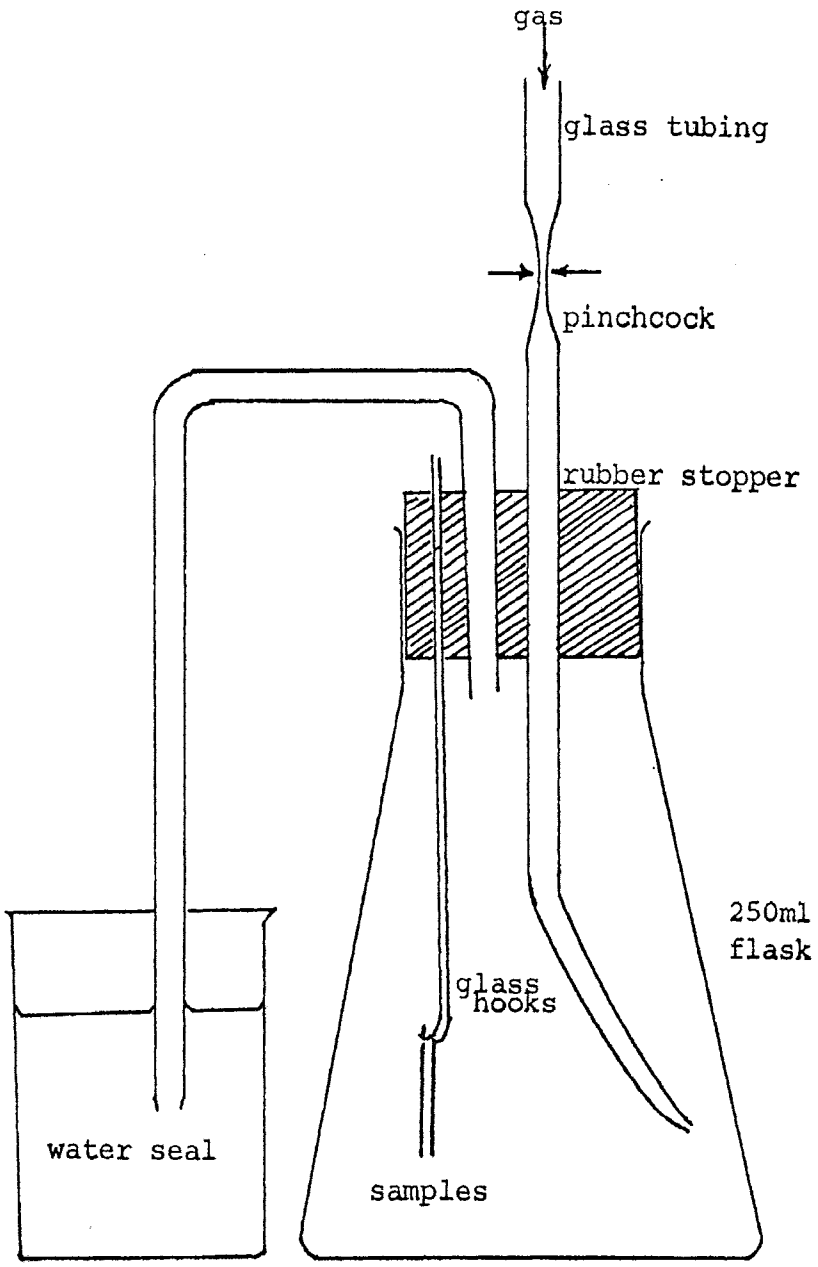

Fig. 3. Corrosion cell for weight loss measurement

rubber stopper. There were two glass hooks and an inlet tubing supplied with a pinchcock for regulating the gas bubbling rate, and a glass cross tubing leading to a water seal. The gas-inlet tube was bent away from the samples as far as possible in order to keep the gas concentration in the solution around the samples more constant. The bubbling rate of the high purity nitrogen or oxygen was approximately 60 bubbles per minute.

Prior to each test, the acid was flushed with the gas at a rapid rate for a period of 30 minutes to saturate the solution with either nitrogen or oxygen. The samples placed on the glass hooks were then immersed into the acid.

At the end of each predetermined interval, the samples were removed, rinsed in distilled water several times and once in acetone. Finally they were dried in vacuum at 100°C, cooled in a desiccator, and carefully weighed.

The apparatus used for investigating the anodic or cathodic polarization behavior of the electrodes is shown in Fig. 4. The electrolytic cell consisted of a spherical 3 necks reaction flask of 500 ml capacity. Rubber stoppers with one or two holes in them fitted into the necks. The first neck served as an inlet and outlet for the gas. The middle one was for the working electrode and the capillary tubing, and the last one for the platinum electrode. The entire assembly was immersed in a water thermostat capable of maintaining the temperature within ± 0.1°C. The capillary tip during the cathodic and anodic potential measurements was kept very close to the working electrode and had a shape to prevent evolved gas on the electrode from entering the capillary.

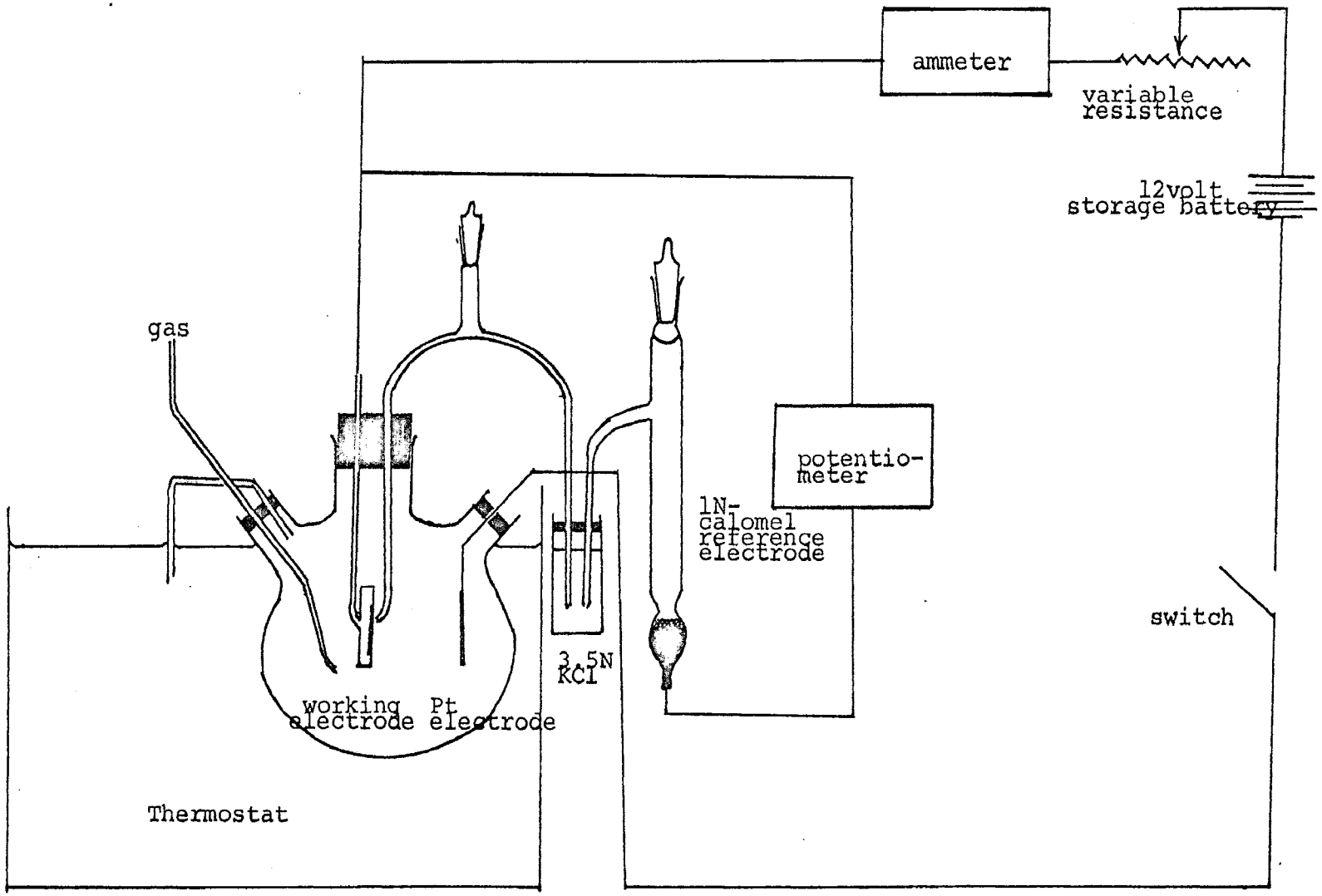

Fig. 4. Apparatus and electrical arrangement for the potential measurement

The solution was stirred by nitrogen gas which was bubbled through the solution.

The electrical wiring used for the potential measurements is shown in Fig. 4. The current was supplied by a 12-volt storage battery through a series of variable resistors and was measured by a sensitive d-c ammeter having ranges from 1 micro-ampere to 500 milli-ampere. The potential of the working electrode was measured using a 1N-calomel reference electrode and a potentiometer. The inverted U-shaped tube with a capillary tip was filled with the same electrolyte as that in the flask and connected to the calomel electrode through a salt-bridge containing 3.5N KCl solution.

400 ml of the respective acid was poured into the flask, and ample time was given to reach thermal equilibrium before lowering the working electrode into the electrolyte. At the same time nitrogen was bubbled through the electrolyte at a rapid rate to saturate it. The working electrode was then lowered into the electrolyte while the platinum electrode still remained above the electrolyte. The gas bubbling rate was reduced to the normal speed, and potential measurements were started, first without external current passing through the electrolytic cell.

Generally, it took about 12 hours for the electrode to reach a steady value for the corrosion potential. When this potential was attained, the platinum electrode was lowered into the electrolyte to act as an auxiliary electrode. The respective circuit was closed by a switch, delivering the prescribed constant current to the cell. Now the potential of the working electrode was measured

at five minute intervals, taking three readings for each constant current. Then the current was increased to another constant value and potential measurements were continued. The same procedure was repeated at the increasing values of constant current.

D. Corrosion Rates of Co, Fe, and Co-Fe Alloys by the Weight Loss Method

Corrosion rates here are expressed in milligrams per square decimeter and per day (mdd), and were calculated from:

$$\text{Corrosion Rate} = \Delta W/A \cdot t \qquad (1)$$

where ΔW is the weight loss of the sample in mg, A is the surface area of the sample in dm^2, and t, the time in days.

No corrections were made either for the change with time of the acid concentration, or for the change in the actual surface area of the sample.

The corrosion rates obtained were plotted as a function of time and are given in the text below. In general, the corrosion rate-time curves can be divided into three consecutive periods, namely: induction, steady, and decline period. Fig. 5 is a schematic diagram of this plot.

The corrosion rate of a metal in solution increases with time (induction period) and then reaches a steady value. The metal is corroded through the induction and steady state periods until the rate of corrosion starts to decline.

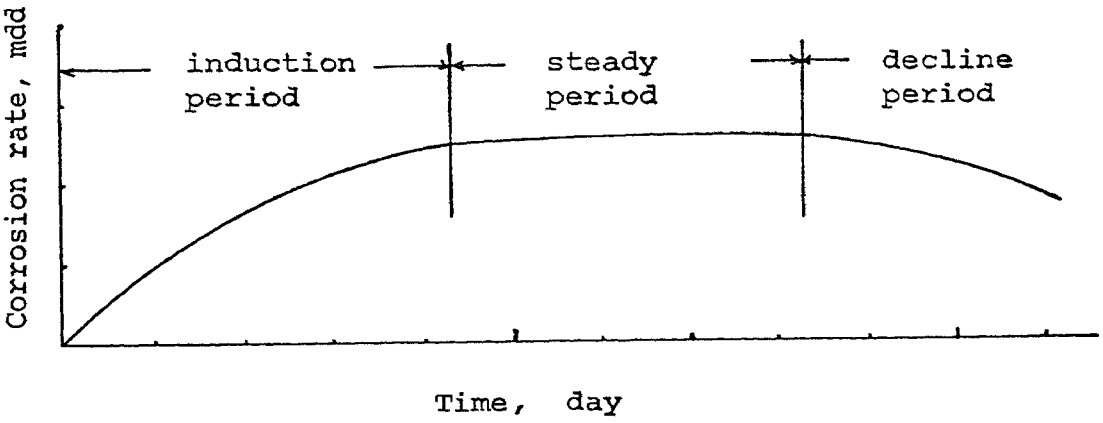

Fig. 5. Typical corrosion rate-time curve

1. Data and results

a. Corrosion rates in H_2SO_4

All the data are summarized in Tables II - Table VII, in the appendix.

(i) Corrosion rate in deaerated H_2SO_4

Fig. 6 gives the corrosion rate-time curve of Co (sintered and sheet), Fe, and 3 Co-Fe alloys in deaerated 1N H_2SO_4. The corrosion rate of pure Fe is about 3.5 times that of pure Co. The corrosion rates are gradually increased as the Fe content of the alloy is increased.

Similar corrosion rate-time curves were also obtained for the same alloys in deaerated 2N and 4N H_2SO_4.

Plots of the steady corrosion rate versus Fe percentage of the Co-Fe alloy, Fig. 7 were obtained. A nearly linear relationship resulted in all cases.

A linear relationship is also found for all the alloys when the steady corrosion rates are plotted against acid concentration, Fig. 8. Fig. 8 also gives a comparison of the corrosion rate produced by sheet Co and sintered Co samples; at the lower acid

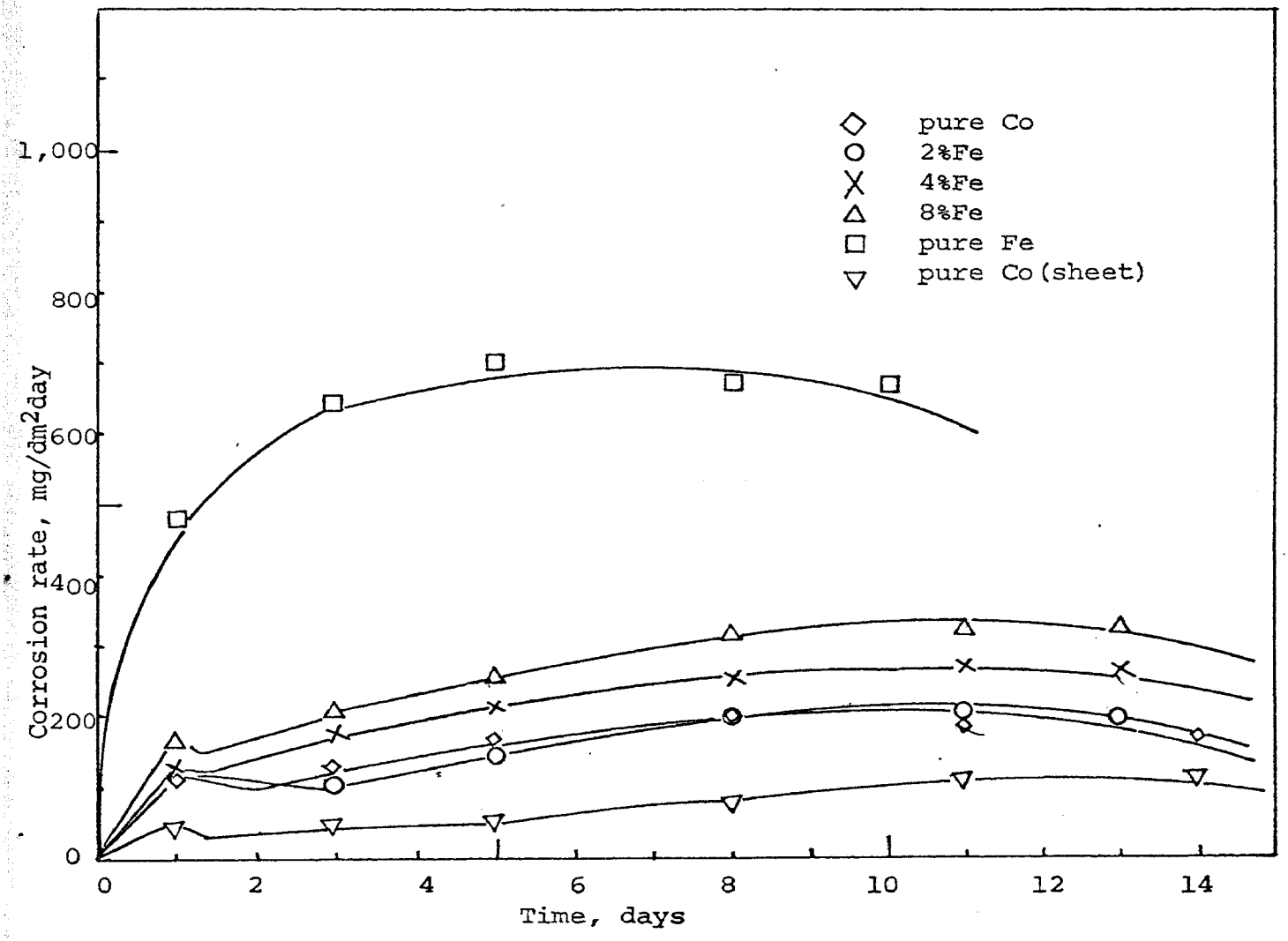

Fig. 6. Corrosion rate-time curves of Co, Fe, and Co-Fe alloys in 1N-deaerated-H_2SO_4

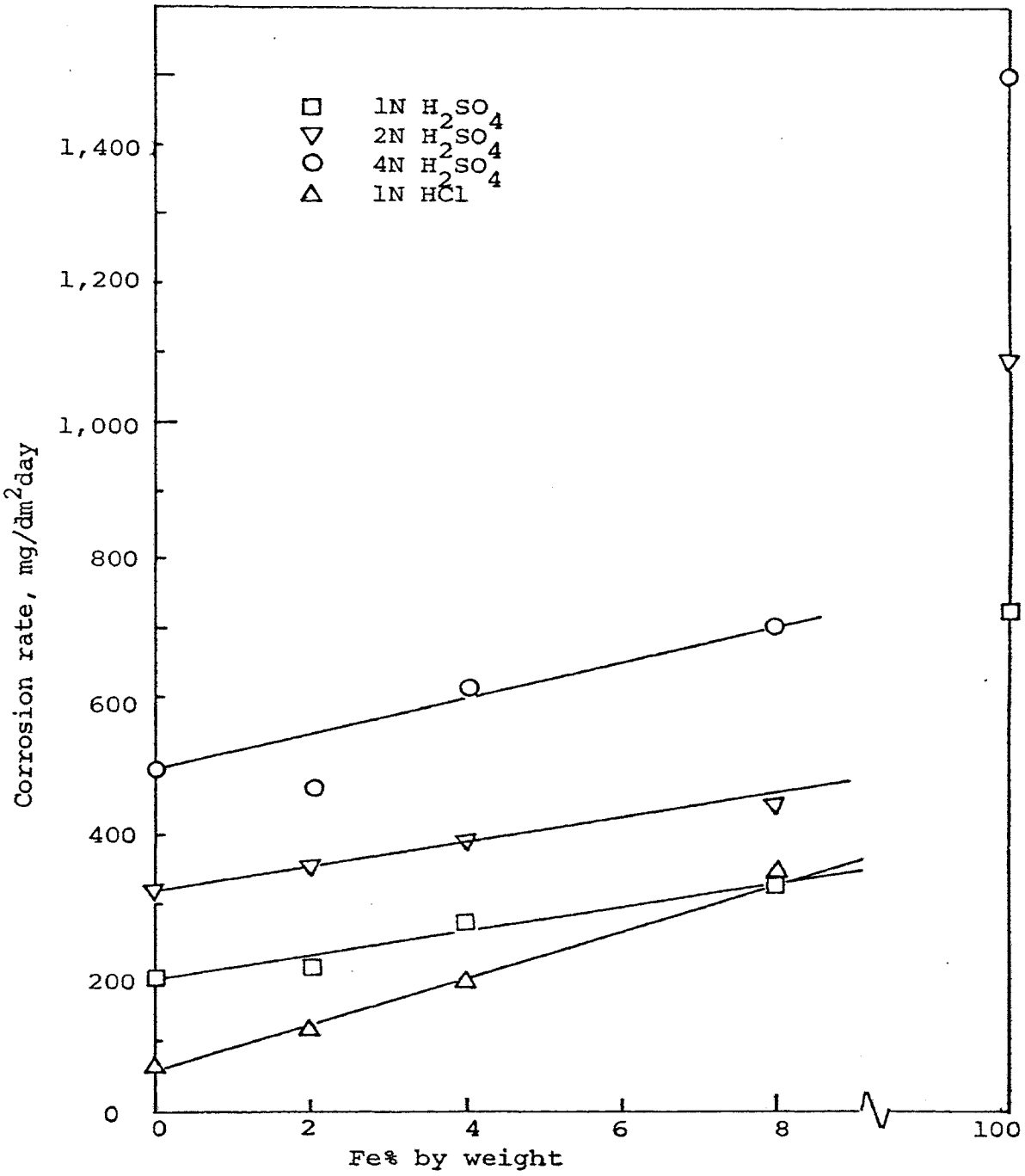

Fig. 7. The effect of Fe content on the corrosion rate of Co-Fe alloys in 4 deaerated acids

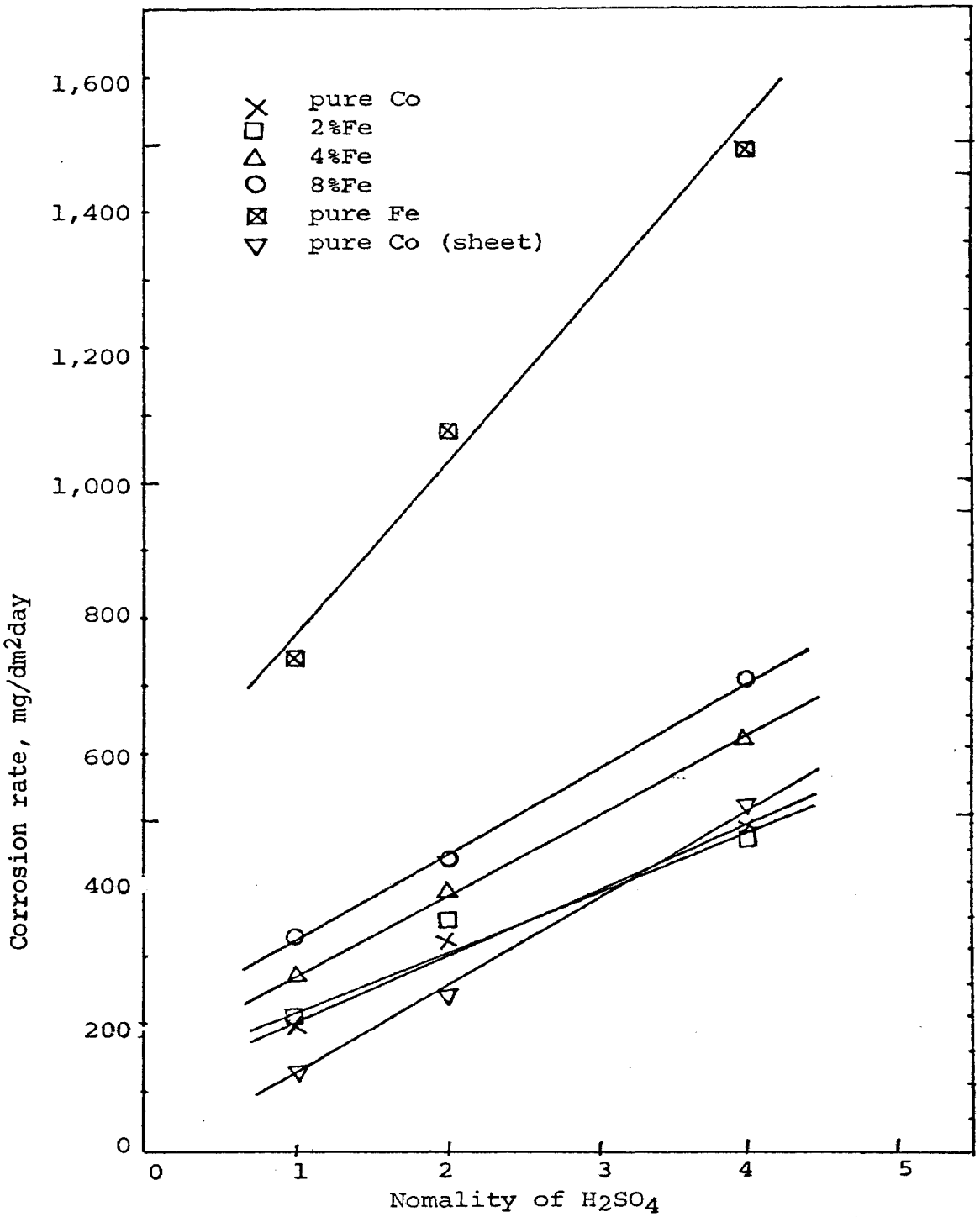

Fig. 8. The effect of deaerated H_2SO_4 concentration on the corrosion rate of Co-Fe alloys

concentrations the corrosion rate of the sintered compact is much greater than that of solid Co, while at higher acid concentrations they approach each other.

(ii) Corrosion rate in oxygenated H_2SO_4

Oxygen generally has a pronounced effect on the corrosion of most metals corroding in non-oxidizing acids. This is also true for the Co and Co-rich Co-Fe alloys in H_2SO_4, where corrosion rates are greatly increased by the presence of oxygen, Fig. 9. However, comparing Fig. 9 with Fig. 6, the corrosion rate of iron in H_2SO_4 is only slightly affected by the oxygen.

To see the effect of Fe content of Co-Fe alloys on the corrosion rate, the corrosion rate-Fe percentage diagram is plotted in Fig. 10: the rate decreases linearly in 1N and 2N H_2SO_4 but increases in 1N HCl and 4N H_2SO_4.

Plotting the corrosion rate of the alloys against the concentration of H_2SO_4, curves of Fig. 11 result. The maximum rate of all four alloys is attained in 2N-oxygenated-H_2SO_4, and in 4N oxygenated acid the rates approach each other. However, for sheet Co the corrosion rate in oxygenated H_2SO_4 is steadily increased with acid concentration.

b. Surface appearance of the corroded samples

The ways sulfuric acid attacked the Co-Fe alloys made by the powder metallurgy method are worthy of mention. In both deaerated and aerated 1N H_2SO_4, the corroding sintered compacts retained their smooth surfaces throughout the entire test. Visual examination revealed no severe attack of the surface, except for a few spots. The metal which dissolved came from the interior of

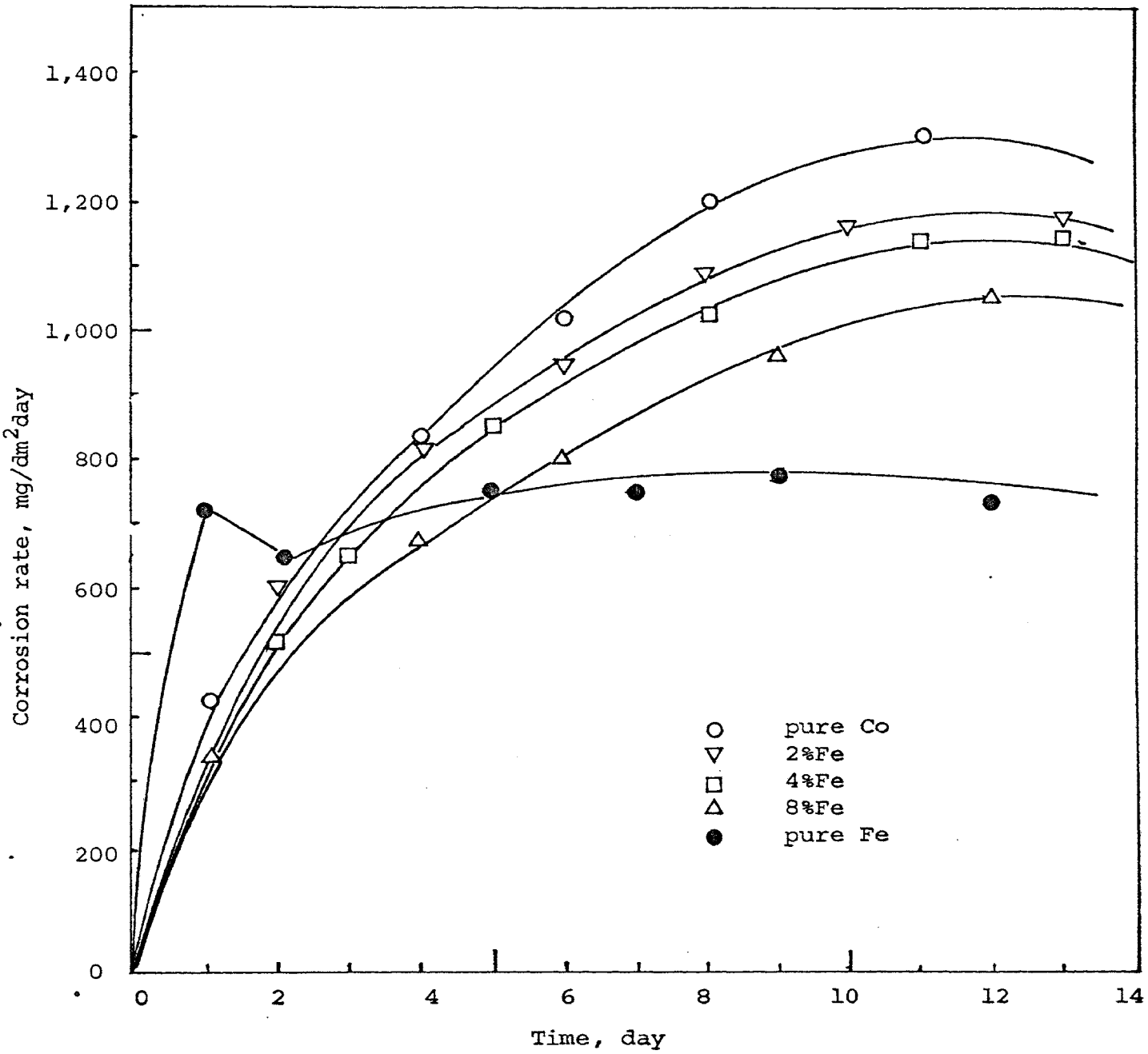

Fig. 9. Corrosion rate-time curves of Co, Fe, and Co-Fe alloys in 1N-oxygenated-H_2SO_4

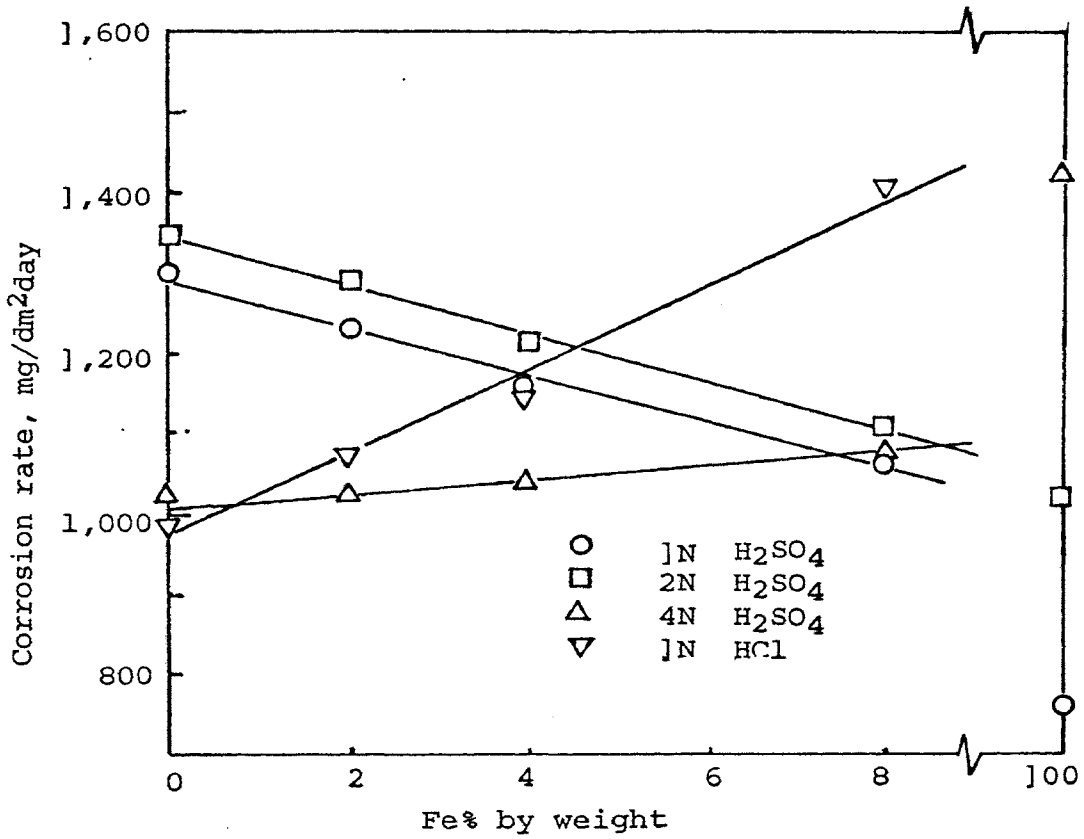

Fig. 1 0. The effect of Fe content on the corrosion rate of Co-Fe alloys in 4 oxygenated acids

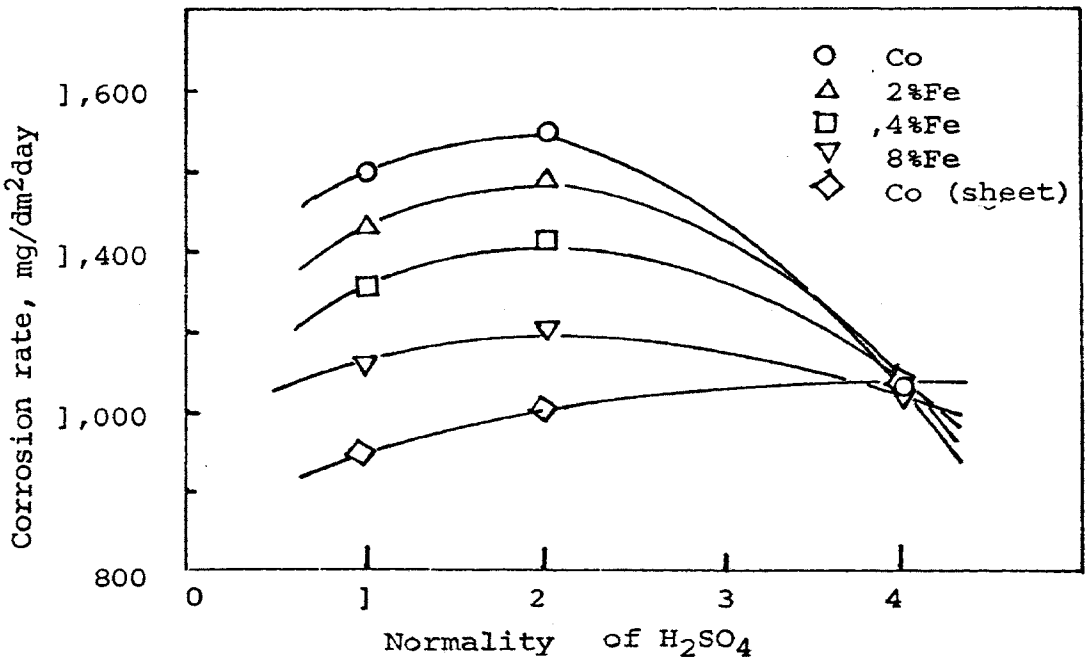

Fig.11. The effect of Oxygenated H_2SO_4 concentration on the corrosion rate of Co-Fe alloys

the sample. Thus, after long exposure to the oxygenated acid (where metal dissolution is large), the samples became porous in the inside while their surfaces remained substantially intact. However, 4N-oxygenated-H_2SO_4 attacked the samples directly on the surfaces; the surfaces of the samples became rough and the samples' dimensions were reduced.

c. Corrosion Rates in HCl

Examination of Figs. 7 and 10 shows that the corrosion rate of Co, and its 2% and 4% Fe alloys is lower in 1N HCl than in 1N H_2SO_4 both in deaerated and oxygenated acids. With higher Fe content, a higher corrosion rate resulted in 1N HCl than in 1N H_2SO_4.

Corrosion rates change linearly with Fe percentage as shown in Figs. 7 and 10. The slopes in the corrosion rate-Fe composition plots reveal that Fe has a more pronounced effect on increasing the corrosion rate of Co-Fe alloys when the alloys are corroded in HCl than in H_2SO_4.

2. The Effect of Temperature on the Corrosion Rate

For many physico-chemical processes, temperature always has a pronounced influence upon the reaction rate. The effect of temperature on the corrosion rate can be expressed in an Arrhenius type equation as given in the following.

$$R_a = A\, e^{-E/RT} \qquad (2)$$

Where R_a is the corrosion rate (mg/dm·day); A is a frequency factor; R is the universal gas constant. Alternatively, log R_a is

a linear function of 1/T. The quantity E, determined from the slope of such a plot, is regarded as the activation energy of dissolution.

a. Data and results

The data for plotting Fig. 12 and Fig. 13 are collected in Tables VIII and IX in the Appendix.

Fig. 12 shows the corrosion rate-time curves, for four temperatures, of sheet Co corroding in deaerated 1N H_2SO_4 ; the induction period and the maximum corrosion rate, respectively, are decreased and increased with increasing temperature. When the logarithm of the maximum corrosion rate at various temperatures is plotted as a function of the reciprocal absolute temperature, straight lines are obtained (Fig. 13).

b. Calculation of the activation energy of dissolution

(i) The activation energy of dissolution of Co in deaerated 1N H_2SO_4 is calculated from the slope of line (i) in Fig. 13.

The slope of line (i) is equal to -4.15×10^3 (deg), thus

$$-\frac{E}{(2.303) \times (1.987)} = -4.15 \times 10^3$$

$$E = 2.303 \times 1.987 \text{ (cal/mole. deg)} \times 4.15 \times 10^3 \text{ (deg)}$$

$$= 1.90 \times 10^4 \text{ cal/mole} = 19.0 \text{ kcal/mole}$$

(ii) The activation energy of dissolution of Co in oxygenated 1N and 2N H_2SO_4 is calculated from the slope of line (ii) and line (iii), respectively.

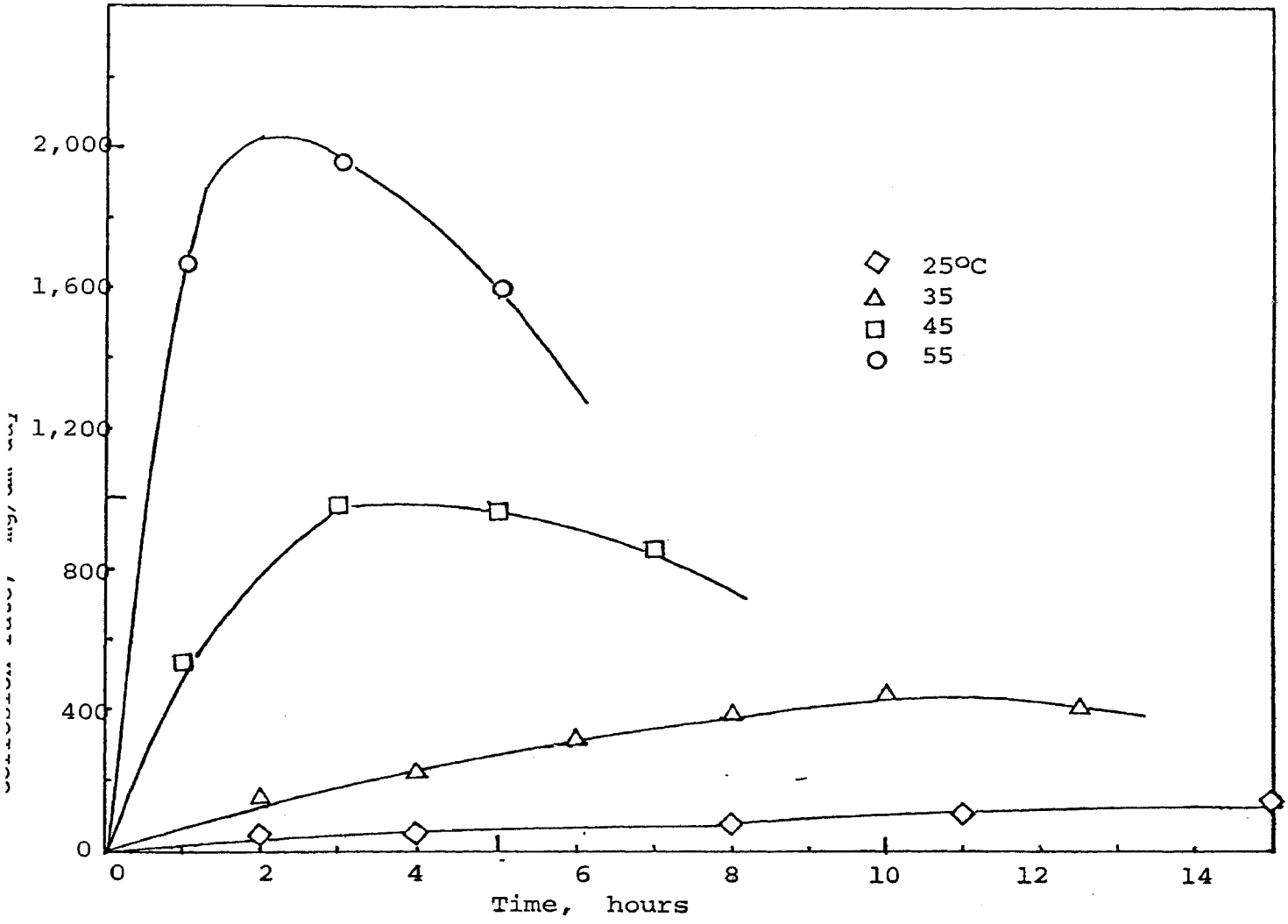

Fig. 12. Corrosion rate-time curves of Co in deaerated 1N-H_2SO_4 at 25°, 35°, 45°, and 55°C

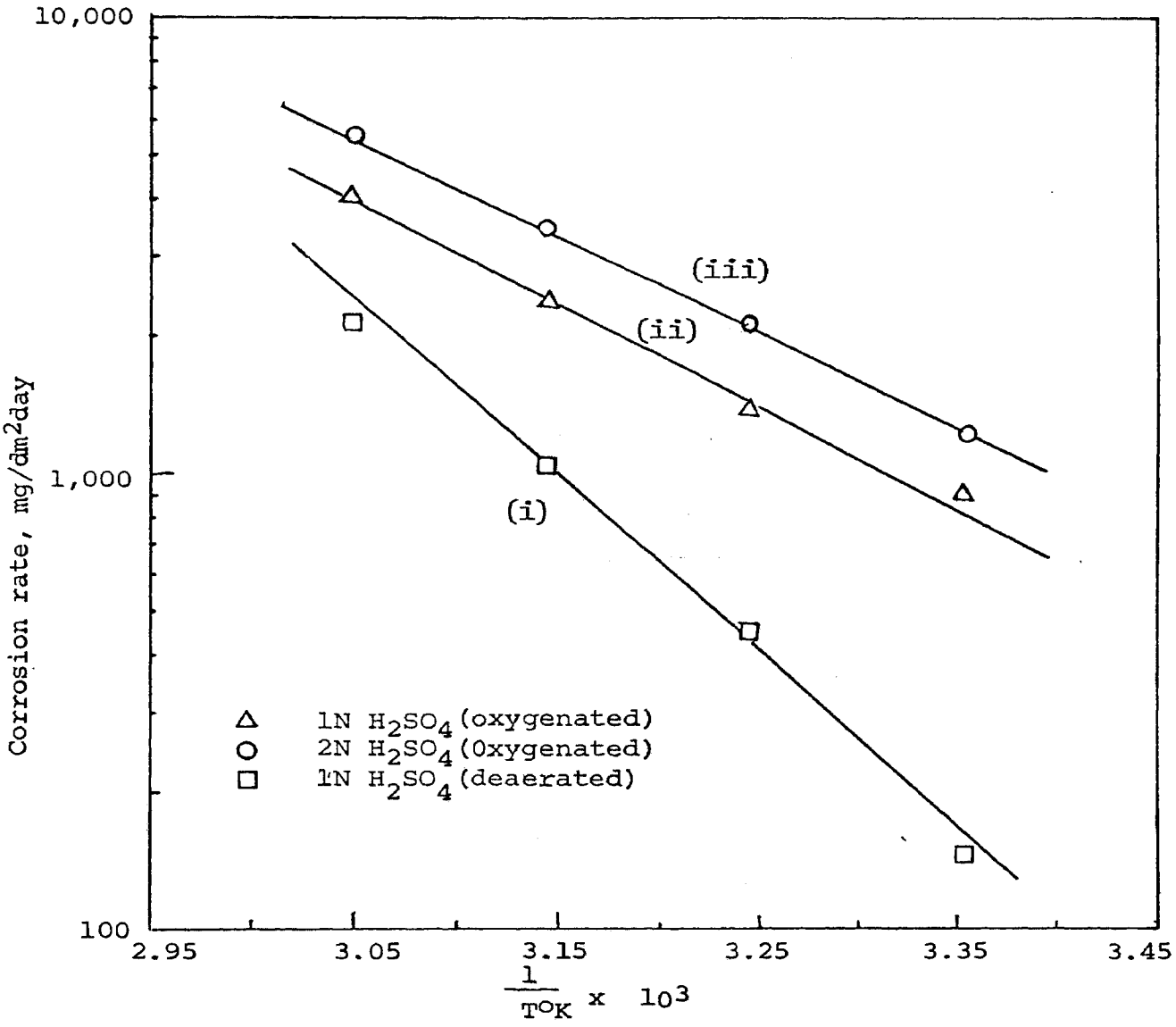

Fig. 13. The effect of temperature on the corrosion rate of Co in H_2SO_4

E_{1N} = 10.3 kcal/mole

E_{2N} = 9.8 kcal/mole

From the above results, it can be seen that the energy barrier for Co to dissolve in deaerated H_2SO_4 is about twice the value of that in oxygenated H_2SO_4.

c. Calculation of temperature coefficient of dissolution

In calculating the temperature coefficient of dissolution reaction, the following relationship was utilized:

$$\text{Temperature coefficient per } 10^{\circ}C = Ra(35)/\ Ra(25) \qquad (6)$$

where Ra(35) is the maximum dissolution rate at 35°C and Ra(25) is the rate at 25°C for the same acid concentration in both cases.

(i) Temperature coefficient of Co in deaerated 1N H_2SO_4 is 430/145 = 2.97

(ii) Temperature coefficient of Co in oxygenated 1N H_2SO_4 is 1400/1020 = 1.37

E. Corrosion Potential of Co, Fe, and Co-Fe Alloys

When the potential of a metal in an electrolyte is measured without applying current, the result is a mixed potential in that electrolyte. The mixed potential of an electrode varies with time and reaches finally the steady corrosion potential.

1. Data and results

The data are shown in Tables X - XIII.

a. Corrosion potential in H_2SO_4

Fig. 14 gives the time-potential behavior of various

alloys in deaerated 1N H_2SO_4. Initially the potential decreases hyperbolically with time and then gradually approaches a steady value (corrosion potential). As the corrosion potential is a function of temperature, the Co (sheet) becomes more active with increasing temperature (Fig. 15). Fig. 16 illustrates the influence of acid concentration on the corrosion potential of sheet Co: the corrosion potential becomes more noble with increasing acid concentration.

b. Corrosion potential in HCl

Similar time-potential curves as those of Fig. 14 were also obtained for various alloys in deaerated HCl.

2. The effect of Fe addition on the corrosion potential of Co-Fe alloys

Iron has a more active corrosion potential than cobalt in acids as is indicated in Fig. 14. When the corrosion potential of the alloy is plotted as a function of Fe content, Fig. 17, it is expected that the curves will shift in the more active direction as the alloy's iron content is increased. It is also shown in Fig. 17 that the corrosion potential of each specific alloy is more active in HCl than in H_2SO_4. However, the corrosion rate measurements, Fig. 7, had shown that Co and its alloys of 2%, 4%, and 8% Fe have higher corrosion rates in H_2SO_4 than in HCl. The comparison of the corrosion rates and corrosion potentials shows that corrosion potentials alone cannot be used to predict the corrosion rates.

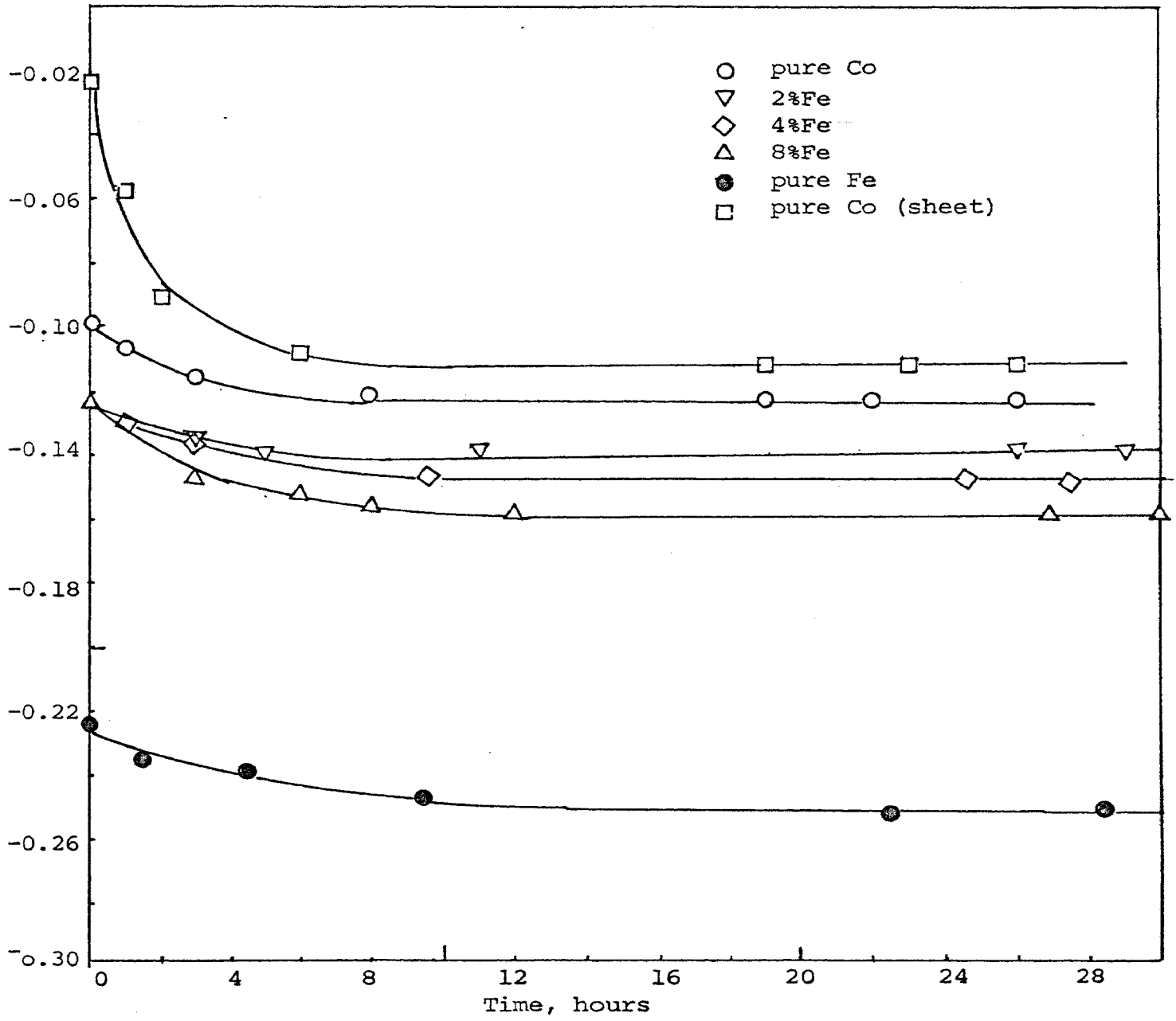

Fig. 14. Potential-time curves of Co, Fe, and Co-Fe alloys in 1N-deaerated-H_2SO_4

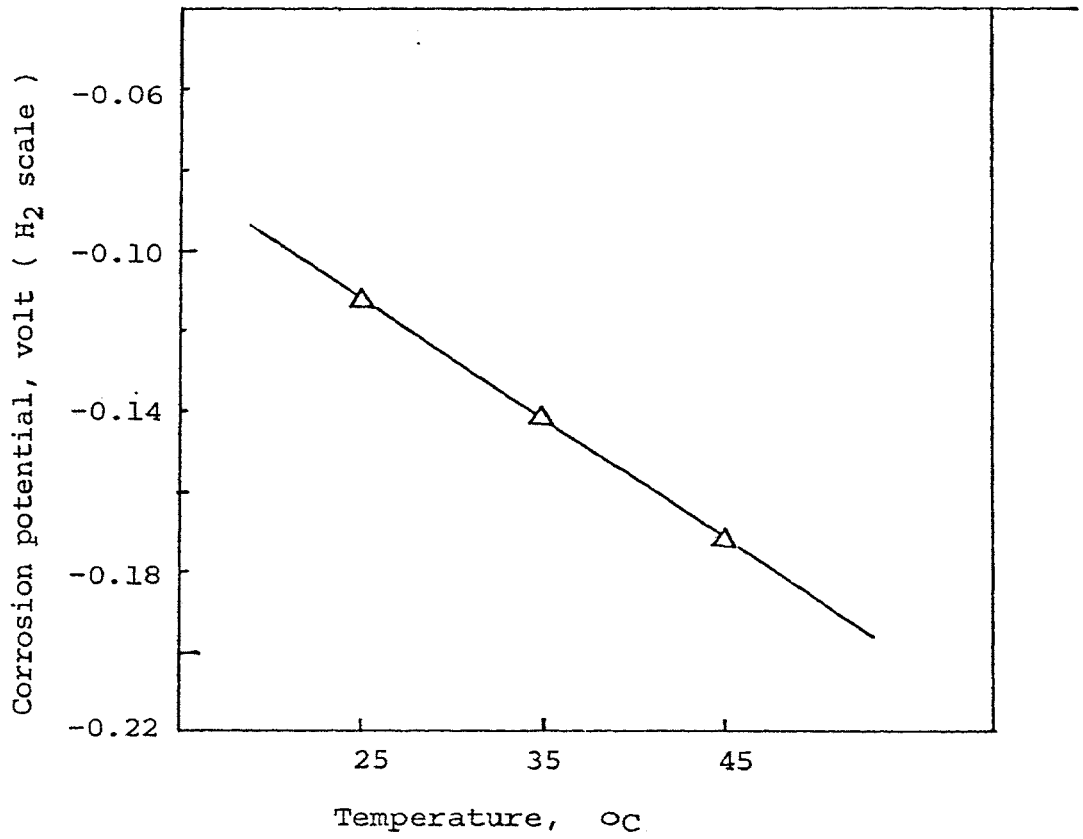

Fig. 15. The effect of temperature on the corrosion potential of Co in deaerated 1N-H_2SO_4

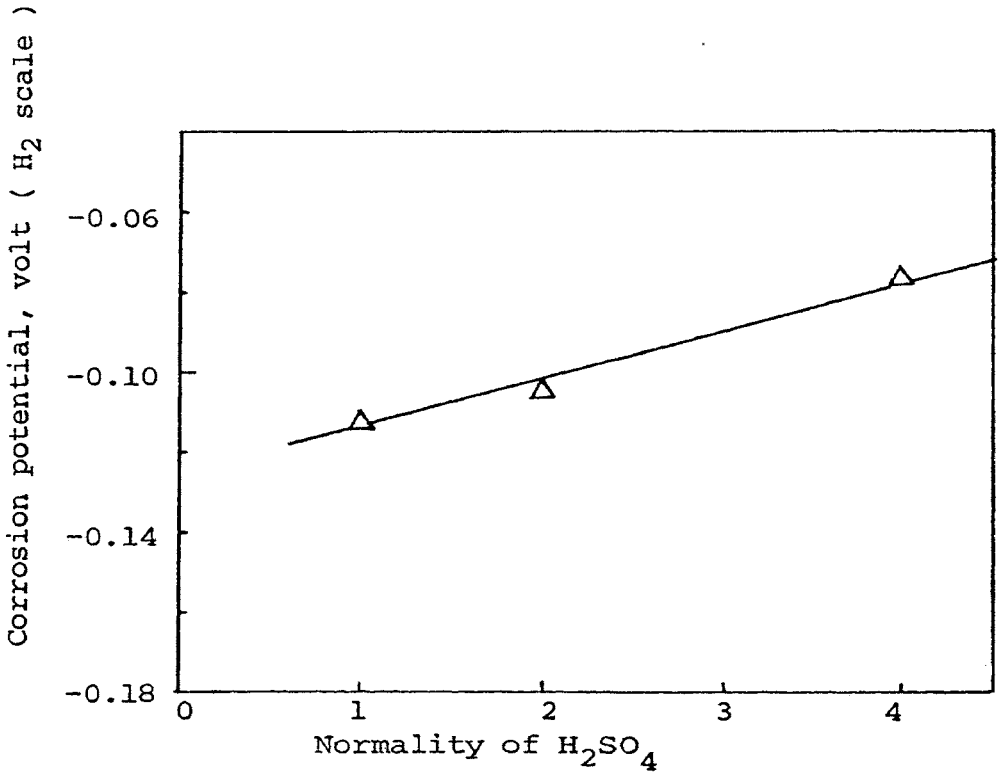

Fig. 16. The effect of H_2SO_4 concentration on the corrosion potential of Co at 25°C

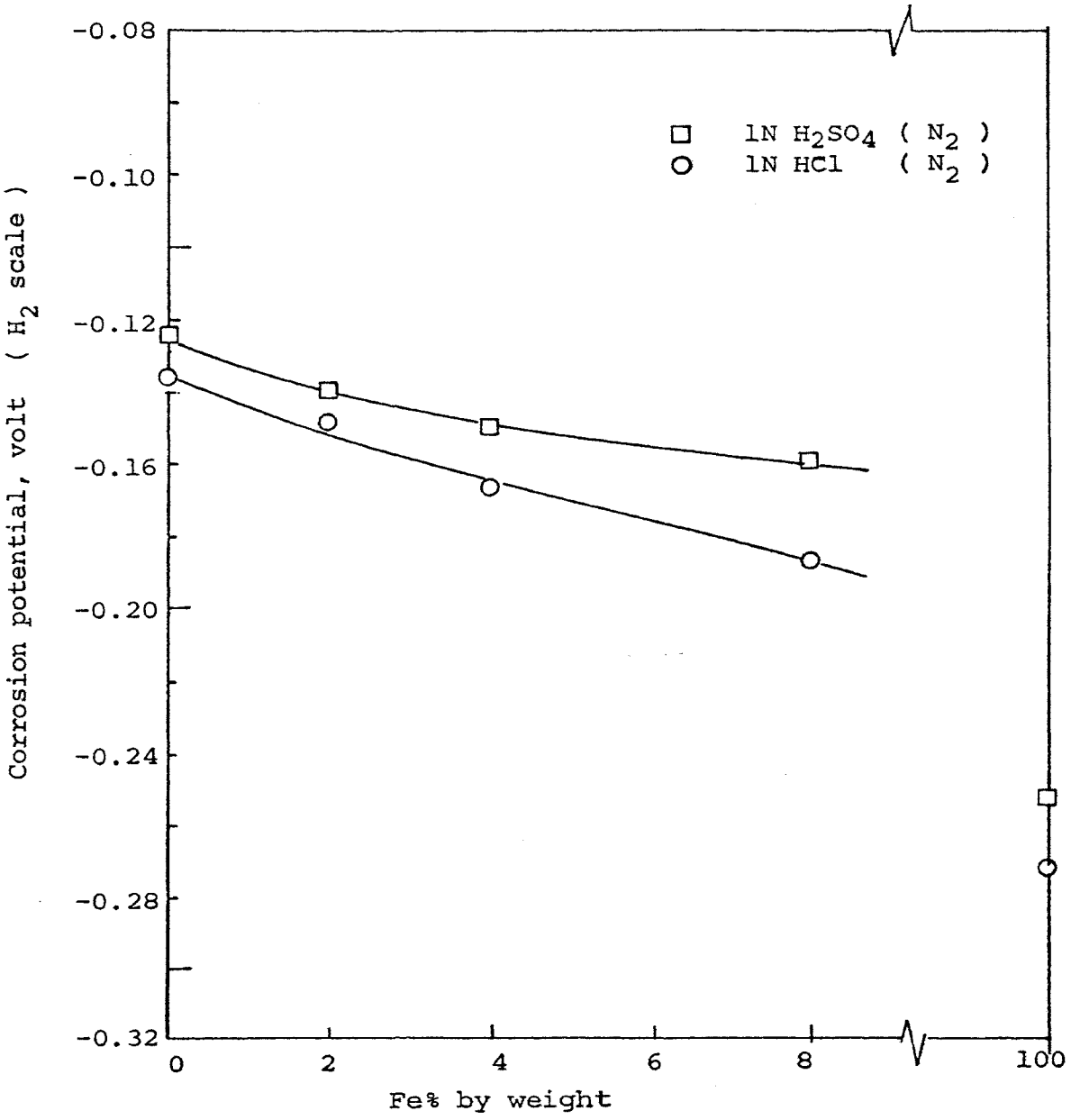

Fig. 17. The effect of Fe concentration on the corrosion potential of Co-Fe alloys in 1N-H_2SO_4 and 1N-HCl

F. Calculation of Corrosion Rates of Co and Co-Fe Alloys from Cathodic Polarization Curves

In the last paragraph it was stated that corrosion potentials alone could not be used to predict the corrosion rates. However, the measurement of corrosion potential along with either the cathodic or anodic polarization behavior of the metal has recently been used as a useful tool for calculating corrosion rates. Cathodic polarization curves are preferred as it is easier to obtain them experimentally. In utilization of this method, the Tafel region of the cathodic polarization curve is extrapolated to the measured corrosion potential to obtain the current which is assumed to be the local action corrosion current. The theoretical basis of this method will be discussed later.

1. Data and results

Cathodic potential measurements are listed in Tables XIV - XVI in the Appendix.

When the cathodic potential is plotted as function of log. current density, the cathodic polarization curve is obtained. Fig. 18 shows four cathodic polarization curves of Co and its alloys with 2%, 4%, and 8% Fe, respectively, in deaerated 1N H_2SO_4. Four horizontal lines corresponding to their respective measured corrosion potentials were drawn. The points of intersection between the corrosion potential lines and the lines extrapolated from the Tafel curve then represent the corrosion current densities of the respective alloys. The corrosion rates in mdd calculated from these corrosion currents are also given on the same diagram.

Fig. 19 presents the cathodic polarization curves of sheet Co in 1N, 2N, and 4N deaerated H_2SO_4. It is observed that the

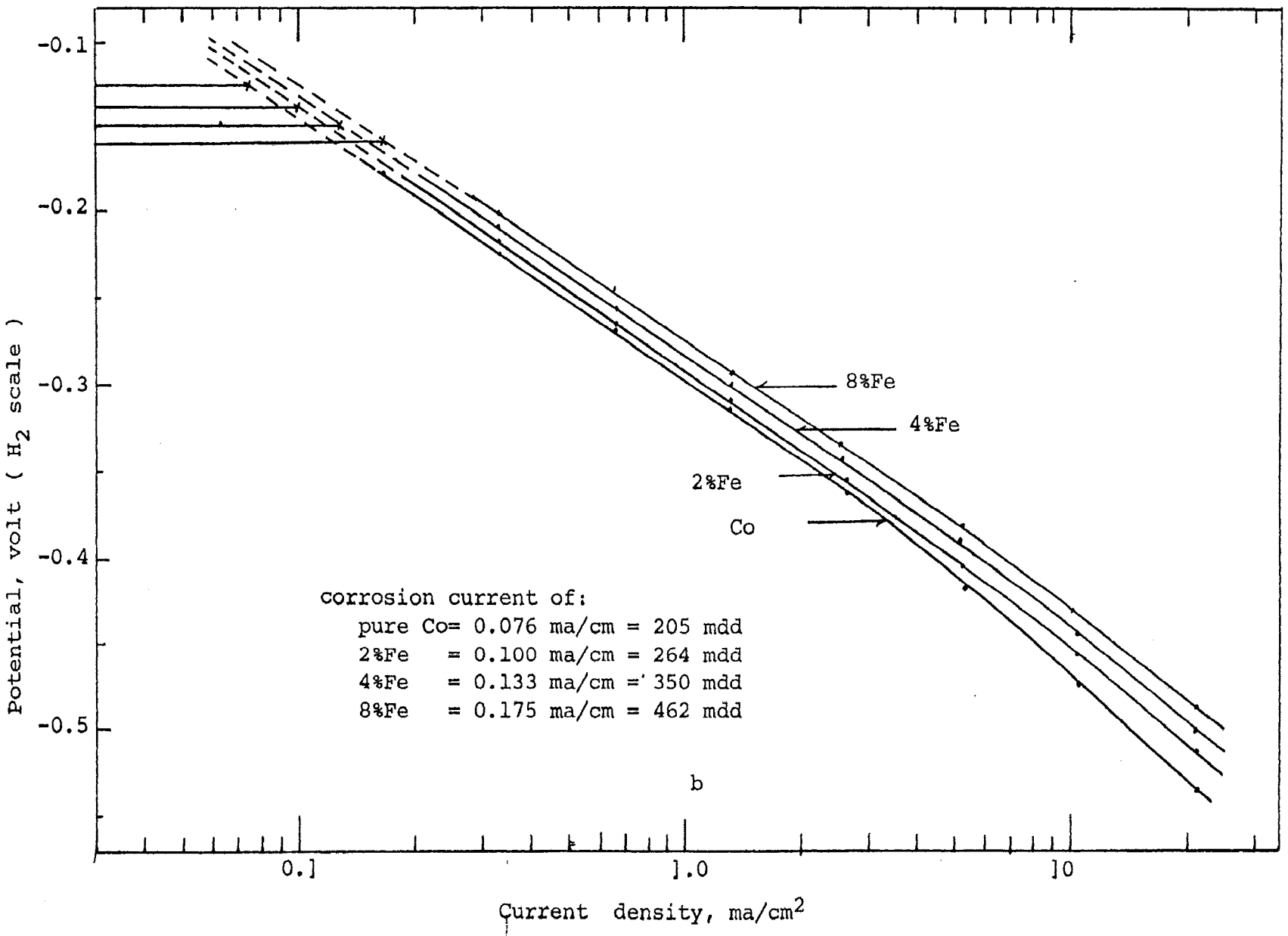

Fig. 18 Cathodic polarization of Co and Co-Fe alloys in 1N H_2SO_4 (deaerated) at 25°C

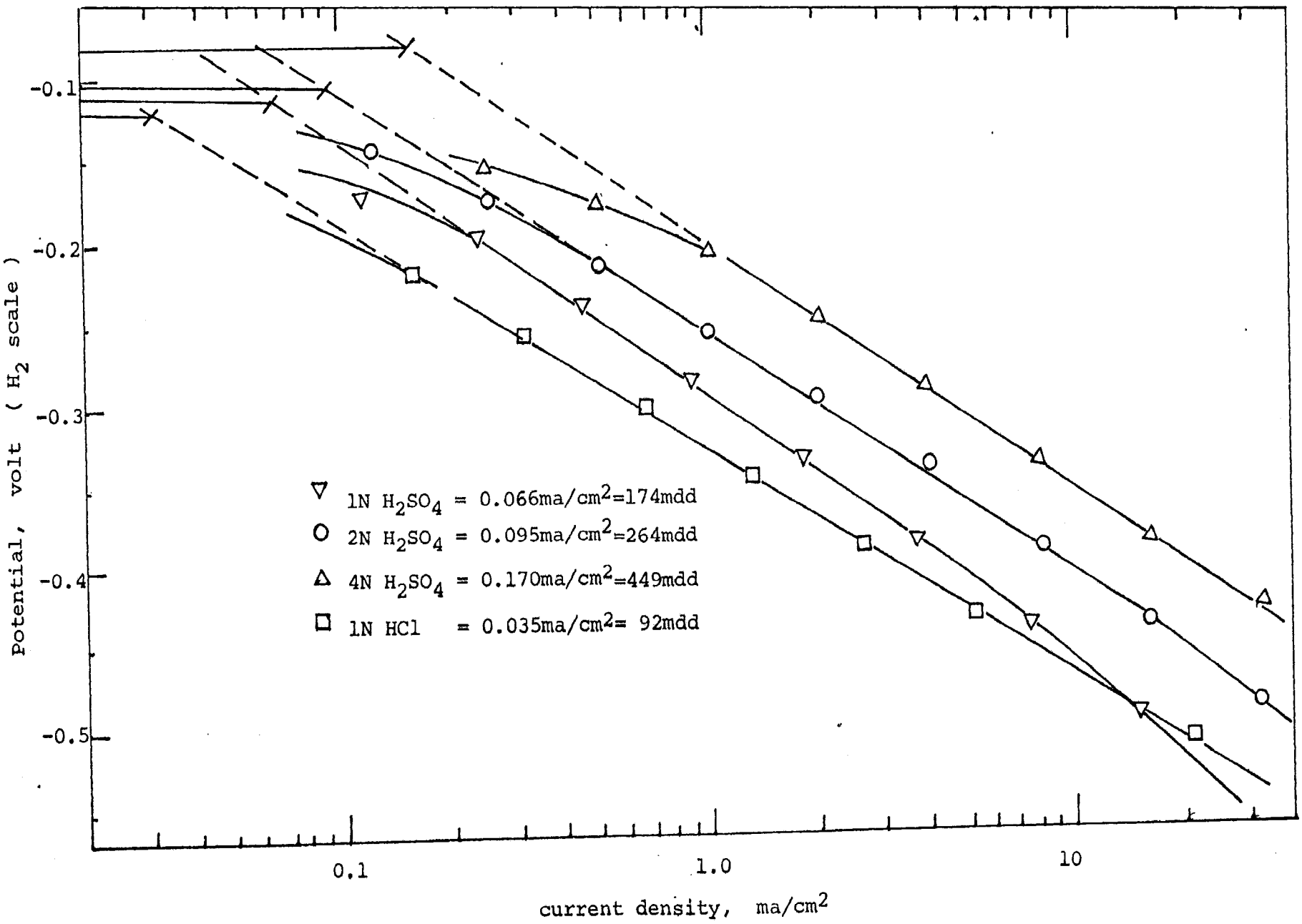

Fig. 19. Cathodic polarization of Co in deaerated 1N, 2N, 4N H_2SO_4 and 1N HCl

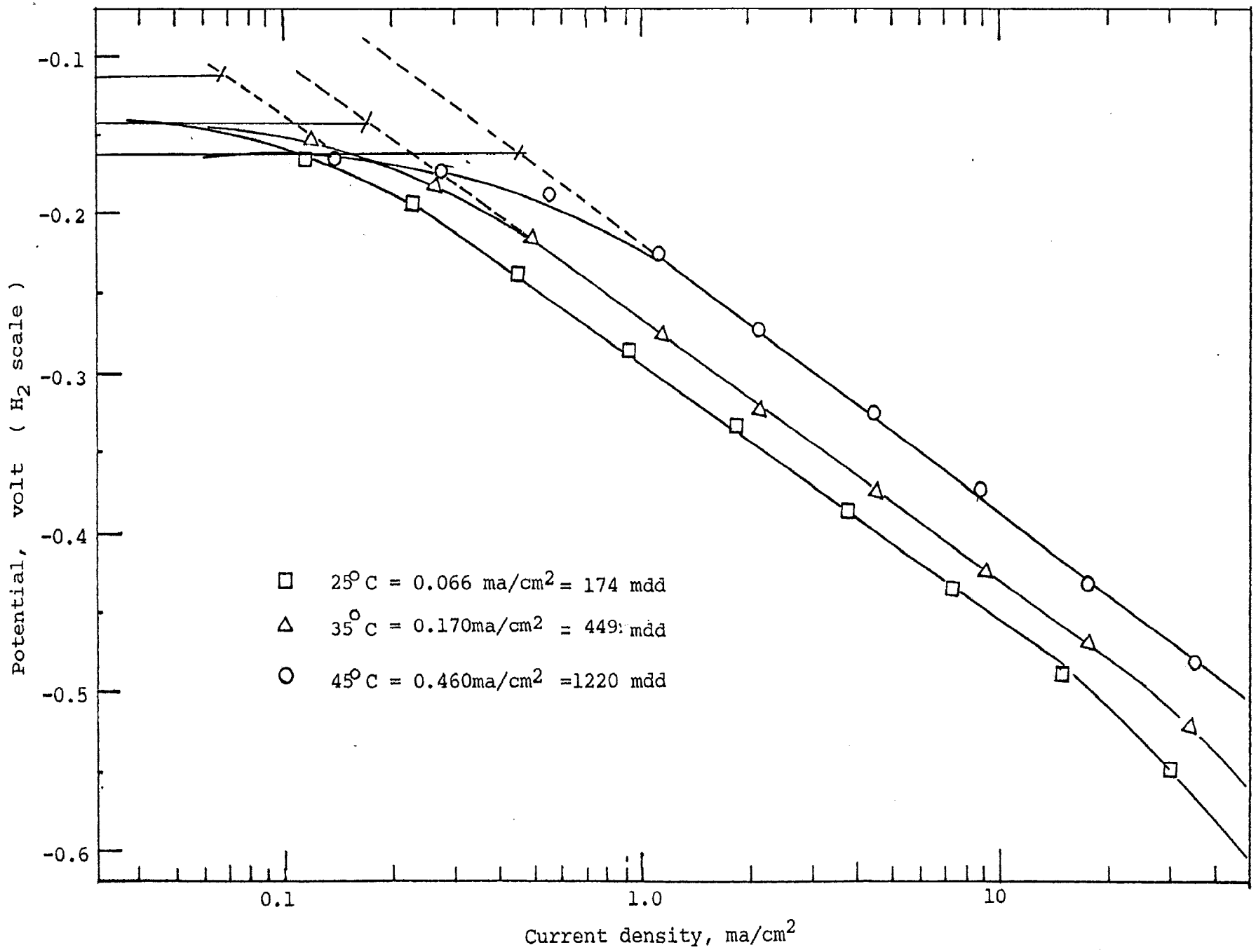

Fig. 20. Cathodic polarization of Co in 1N-deaerated-H_2SO_4 at 25°, 35°, and 45°C

Table I

Comparison of the Corrosion Rates Determined by the Weight Loss Method and the Corrosion Rates Measured by the Electrochemical Method

Metal	Acid	Tempt. °C	Corr. Rate Wt. Loss (i)	Corr. Rate Tafel (ii)	Deviation (ii-i/i)
sheet Co	1N H_2SO_4	25	145	170	+17%
sheet Co	1N H_2SO_4	35	460	470	+2.2%
sheet Co	1N H_2SO_4	45	1020	1250	+23%
sheet Co	2N H_2SO_4	25	235	265	+13%
sheet Co	4N H_2SO_4	25	515	449	-13%
sheet Co	1N HCl	25	83	92	+11%
sinter Co	1N H_2SO_4	25	195	205	+5%
98% Co	1N H_2SO_4	25	205	264	+29%
96% Co	1N H_2SO_4	25	275	350	+27%
92% Co	1N H_2SO_4	25	330	462	+40%

increase of acid concentration causes the cathodic polarization curve to shift in the more noble (cathodic) direction. The cathodic polarization curve of sheet Co in deaerated 1N HCl is also shown in Fig. 18; the corrosion current is obviously lower than that of Co in 1N H_2SO.

Temperature also shifts the cathodic polarization curve to the more noble direction, Fig. 20. although the corrosion potential becomes more active when temperature is raised (Fig. 15).

2. Comparison of the corrosion rates obtained by the weight loss method and by the electrochemical method

Table I lists the corrosion rates obtained by both methods. Comparison of these results shows that the corrosion rates calculated from Tafel curves are higher throughout, with one exception, than the values determined by the weight loss method. However, this deviation is acceptable.

G. Anodic Polarization and Passivation of Co, Fe, and Co-Fe Alloys

Application of an anodic current to a corroding metal causes a potential shift in a more noble direction and usually the total corrosion rate increases with current. This continues until, with metals exhibiting passive behavior, a certain current density, I_{crit}, is reached. If the applied current is increased beyond I_{crit}, the potential shifts rapidly in the more noble direction. At the same time the corrosion rate decreases markedly and the metal is said to go passive.

Experimental measurements of anodic polarization potential are more difficult to carry out than those of cathodic

polarization potential; the potential fluctuates with time and usually takes longer to reach a steady value.

1. Data and results

The anodic potentials necessary for plotting Fig. 21 are listed in Table XVIII in the Appendix.

Fig. 21 shows the anodic polarization curves of Co and Fe. For Co, the critical passivation current density, I_{crit}, is around 320 to 350 ma/cm^2 in nitrogen-purged 1N H_2SO_4. Fe passivates at a little higher current density than Co in the same solution (at about 400 to 430 ma/cm^2). It is difficult to set out the relationship of I_{crit} and Fe content of the Co-Fe alloy. However, the general tendency is that I_{crit} increases slightly with increasing Fe concentration of the Co-Fe alloys.

The stirring rate of the solution influences I_{crit} of a specific metal. This is shown by a decrease of I_{crit} of a Co anode in 1N H_2SO_4 with no nitrogen bubbling; the only form of stirring mechanism then was by the hydrogen evolution and the convection caused by current flowing. In 1N HCl, the Co anode did not become passive even up to a current density of 800 ma/cm^2.

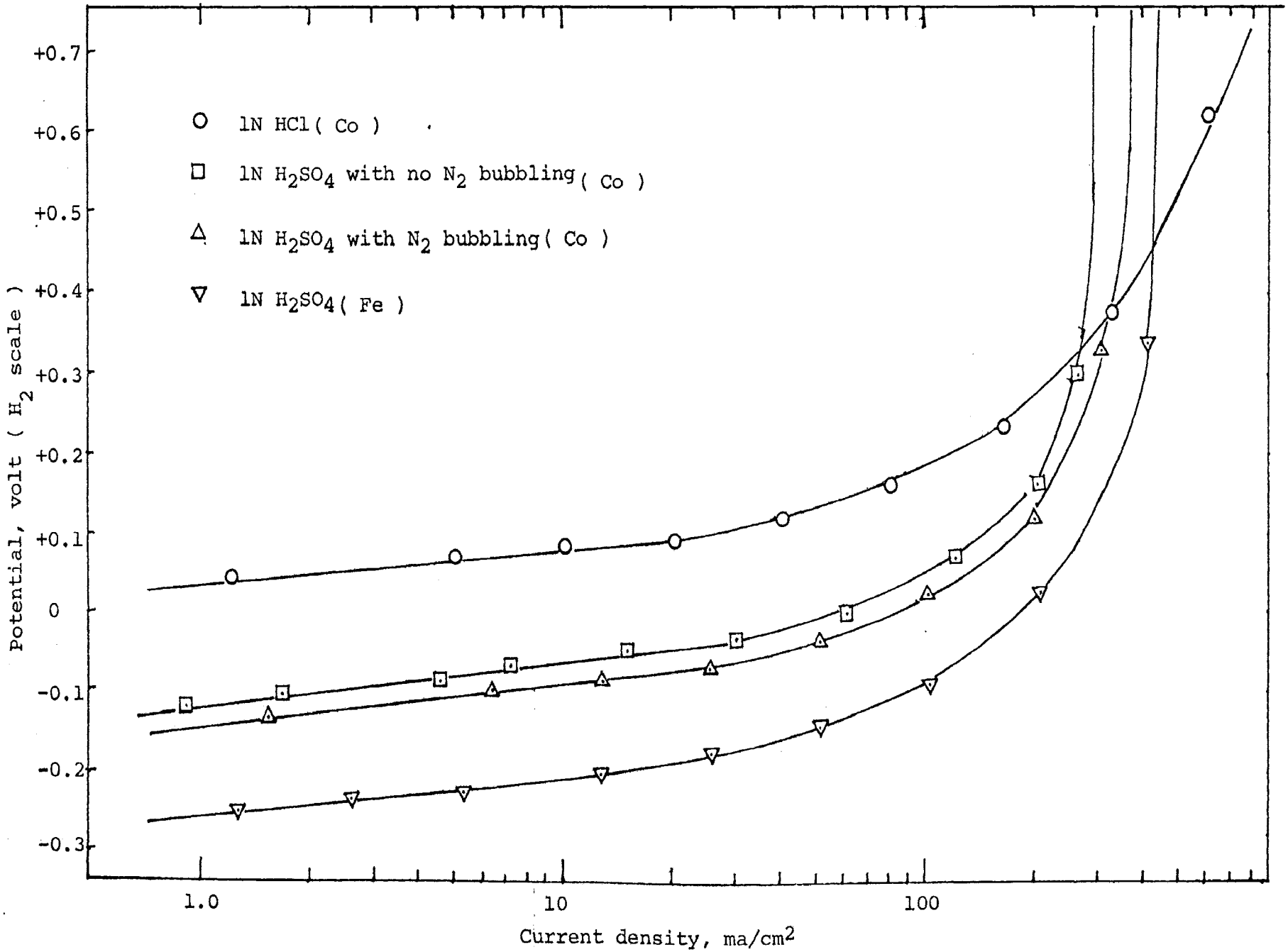

Fig. 21. Anodic polarization of Co and Fe in 1N H_2SO_4 and 1N HCl

IV. DISCUSSION

A. Corrosion of Co and Co-Fe Alloys in Acids

1. Introduction

a. Tendency of a metal to corrode

Most metals exist in nature in a combined state. Their ores or natural compounds must be subjected to pyrometallurgy and chemical refining involving an addition of energy to bring them into a metallic state. It follows that the metallic state represents a condition of higher energy content. It is to be expected that the natural tendency of metals is to combine with other elements and to revert to a lower energy state with a corresponding release of energy. This decrease in free energy is the driving force of the corrosion reaction.

b. The electrochemical nature of corrosion

Corrosion of metals in aqueous solution is electrochemical in nature.[13,14,15] The electrochemical theory states that metals corrode by formation of local cells on their surfaces. The cells consist of anodic areas, where solution (corrosion) of the metal occurs, and cathodic areas, where there is a corresponding reduction. To illustrate, the corrosion of a divalent metal in an deaerated acid can be described as follows:

$$\text{Anodic reaction} \quad M \longrightarrow M^{++} + 2e \tag{1}$$

$$\text{Cathodic reaction} \quad 2H^{+} + 2e \longrightarrow 2H_{ads} \longrightarrow H_2 \tag{2}$$

The rate of electrochemical corrosion is determined by the flow of current, which is produced by the potential difference between

the anodic and cathodic sites. The circuit works by the transference of ions through the solution.

When corrosion occurs, there is a reduction of hydrogen ions (Eq. 2). For this reduction an activation energy is usually required.[16] This causes a change in cathodic potential which can be expressed by

$$\eta = - \beta_H \log i \qquad (3)$$

where η is the overvoltage, β_H is a constant (Tafel constant) and i is the current equivalent to the rate of reduction. Eq. 3 is known as the Tafel equation. If the potential is plotted against the logarithm of current (density) and if there are no side reactions, a straight line results. This straight line HC_1 is shown in Fig. 22 and is called the cathodic polarization curve.

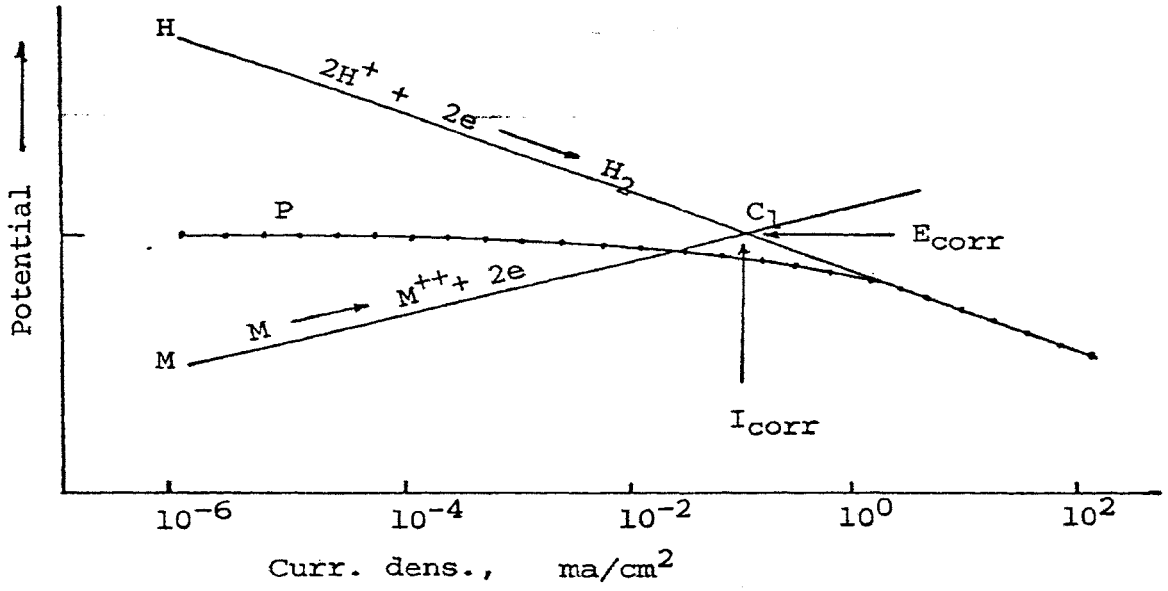

Fig. 22. Polarization diagram of a corroding metal system

When corrosion occurs, there is also oxidation of the metal (Eq. 1). The anodic reaction results again in a polarization curve

which in a plot of potential vs. log i frequently results in a straight line MC_1 (Fig. 22).

Point C_1 is the intersection of the anodic and cathodic polarization curves. At this point the rate of anodic reaction of a corroding metal is equal to the rate of cathodic reaction. This, according to Evans[17], gives the steady-state potential, E_{corr}, and corrosion current, I_c, of the corrosion system.

Experimentally, however, the individual oxidation curve (MC_1) or reduction curve (HC_1) of an active metal cannot be measured. When an external current is impressed on a corroding metal, the total cathodic current density in Eq. 3 should be replaced by the sum of two terms: i_x, the external applied cathodic current and $i_{l.a.}$, the local action current. The two are obviously not independent of each other since cathodic protection is based on the decrease of i_{la} with increase of i_x. From what has been described above, Equation 3 may be written in a more general form:-

$$\eta = - \beta_H \log(i_x + i_{la}) \qquad (4)$$

Eq. 4 is consistent with the horizontal portion of the experimenta curve (P in Fig. 22) since it predicts that the potential will not change significantly until the external current approaches values of the same order of magnitude of the local action current. It is important to note that with no external applied current ($i_x = 0$), η is equal to the corrosion potential E_{corr}, on the hydrogen overvoltage scale, and i_{la} equals the corrosion current; hence

$$E_{corr} = -\beta_H \log I_{corr} \quad (5)$$

Referring to both Eq. 4 and Fig. 22, it is apparent that at relatively high applied current densities, the applied current begins to approach total actual cathodic current, since the corresponding local action current becomes negligible. Thus curve P fall on the hydrogen reduction curve when the applied cathodic current reaches a magnitude of several times the corrosion current.

2. Mechanism of the corrosion reaction

The rate at which a metal corrodes in a deaerated acid will be governed by the slowest reaction or step occurring in the mechanism of the dissolution of the metal. In the solution of Co and Co-Fe alloys there are several stages that may control the corrosion rate:

(1) The anodic reaction $M \longrightarrow M^{++} + 2e$.

(2) Diffusion of hydrogen ions (or H_3O^+) to the local cathodes.

(3) Discharge of H^+ with formation of adsorbed hydrogen atoms $H^+ + e \longrightarrow H_{ads}$.

(4) Recombination of the hydrogen atoms $H_{ads} + H_{ads} = H_2$.

(5) Diffusion of hydrogen molecules from the cathodes.

If the rate is governed by (2) and (5) the reaction is said to be diffusion controlled. If, however, the slowest reaction is step (1) or (3) and (4), then the controlling mechanism is electrochemical. Copson[18] states that a rate increases of 100 to 200 per cent per 10 degree centigrade increment are typical of the chemical (or electrochemical) reaction, and rate increases of 20 to 30 per cent per 10 degree rise are typical of the diffusion

controlled processes. The result of the present investigation showed a temperature coefficient of 2.97 for Co corroding in deaerated H_2SO_4. Therefore, the governing mechanism is electrochemical as given by (1), (3), and (4). Referring to Fig. 12, it can be seen that the induction period and the maximum corrosion rate of Co corroding in deaerated H_2SO_4, respectively, decreases and increases with increasing temperature. The induction period is defined as the time required for the metal to reach the maximum corrosion rate, which evidently is related to the exposure of cathodic sites to the corrosive solution. The greater maximum corrosion rate at higher temperature is due not only to the increasing total cathodic areas but also due to the reduced hydrogen overvoltage. From the discussion above, it can be concluded that the controlling mechanism should be steps (3) and (4), i.e. corrosion of Co and Co rich Co-Fe alloys are cathodically controll

3. Corrosion of Co and Co-Fe alloys in oxygenated acids

a. Influence of oxygen

The first step in the cathodic corrosion reaction is the discharge of H^+ with formation of adsorbed hydrogen atoms on the local cathodes. It is to be expected that a reagent which reacts with the atomic hydrogen would accelerate the corrosion rate. Oxygen, which is an oxidizer, does it. However, corrosion of Co in aerated acid may be diffusion controlled as the temperature coefficient is only 1.37. The removal of hydrogen atoms proceeds in the following way:

$$2H + 1/2\ O_2 \longrightarrow H_2O \qquad (6)$$

The rate is then governed by the rate of arrival of O_2 at local cathodes. Oxygen acts as a cathodic depolarizer, and thus increases the corrosion rate. Experiments conducted with pure Co and Co rich Co-Fe alloys corroding in H_2SO_4 and HCl show again that oxygen has greatly increased the corrosion (comparing Fig. 11 with Fig. 8).

b. Explanation of the different types of attack to Co-Fe alloys in oxygenated H_2SO_4

It is mentioned in the previous chapter that the corroded Co and Co-rich Co-Fe alloys corroding in oxygenated 1N H_2SO_4 had porous structures inside whereas the surfaces of the sample showed no appreciable attack. However, a 4N-oxygenated-H_2SO_4 attacked the same alloys at their surfaces.

To explain these phenomena, it has to be emphasized that the samples were sintered compacts prepared by the powder metallurgy method in a hydrogen atmosphere. It seemed that these sintered compacts possessed a more corrosion resistant surface layer than the interior. This is probably due to:

(1) The smaller amount of carbon or carbide (which usually is a low hydrogen overvoltage site) at the surface layer due to decarbonization of the alloys in hydrogen.

(2) The samples acquired a more dense surface layer than the interior body due to surface grinding and polishing, forcing the metal to flow and close the exits of the pores in the samples.

In a comparatively weak acid (1N H_2SO_4), the surface of the sample was relatively stable. But in oxygenated solution, pits are apt to form which would enable the solution to penetrate into the interior of the sample. The less corrosion resistant alloy inside would then dissolve more easily and, hence, become porous inside while the surface of the sample remained nearly intact.

When the corrosive ability of the acid became strong enough (4N H_2SO_4) to dissolve the corrosion resistant layer, attack would then proceed from the surface.

c. Explanation of the decline of corrosion rates of Co and Co-Fe alloys at higher oxygenated H_2SO_4 Conc.

Fig. 11 shows a maximum corrosion rate for all the alloys in oxygenated 2N H_2SO_4: the corrosion rate of the same alloy is higher in 1N H_2SO_4 than in 4N H_2SO_4. Although 4N H_2SO_4 is more corrosive, the formation of the porous structure of the samples in 1N and 2N H_2SO_4 was probably the main reason accounting for the higher calculated corrosion rates. The porous structure exposes a much larger area of the sample to the solution and, hence, the weight loss is greater.

The nominal corrosion rate, calculated by dividing the weight loss of the sample by the macroscopic surface area, was, therefore, higher for the alloy corroding in 1N H_2SO_4 than in 4N H_2SO_4.

The corrosion of sheet Co occurred always from the surface despite the concentration of H_2SO_4. The steady increase of corrosion rate of sheet Co with increasing acid concentration, and the lower corrosion rate of sheet Co than the sintered Co in 1N and 2N H_2SO_4 but attaining about the same rate in 4N H_2SO_4 seems to be accounted for by the above explanation.

B. Calculation of the Corrosion Rates by the Tafel Extrapolation Method

Table I shows that the corrosion rates calculated by using the Tafel extrapolation lines have higher values than those determined by the weight loss method. The result is quite expected and can be discussed by using plots of potential-current diagrams as illustrated in Fig. 23.

In Fig. 23A, the calculated corrosion current density is given by point C', which is obtained by extrapolating the cathodic polarization curve from the Tafel region to the corrosion potential E_{corr}. However, in an actual corrosion system, an EMF equal to $(E_c - E_a)$ should exist in order to push a corrosion current, I_c, over the resistance of the solution. According to Fig. 23A the actual corrosion current, I_c, is obviously less than the value, I'_c, indicated by point C'.

In addition, the measurement of the activation hydrogen overvoltage (η in the Tafel equation) may be complicated by two interferring phenomena--concentration polarization and resistance drop effects--especially when the current becomes relatively large. The cathode will be polarized more and thus deviate appreciably from the Tafel behavior if the above two factors become large.

Fig. 23B shows points deviating from the Tafel behavior which is plotted as a solid line, caused by concentration and resistance polarization. If a straight line is plotted through these points and extrapolated, then a higher corrosion current results (I_c'' instead of I_c').

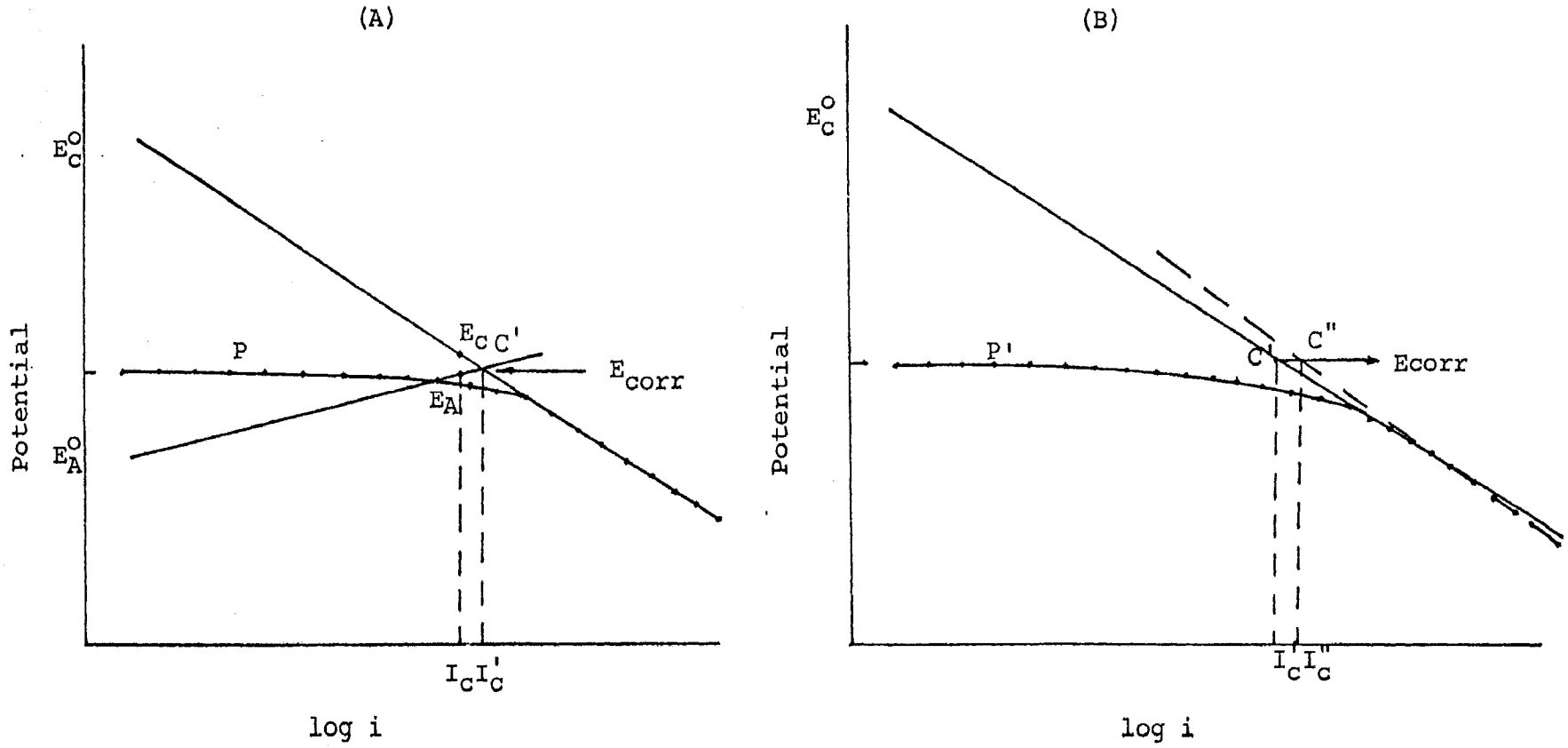

Fig. 23. Schematic polarization curves illustrating why the corrosion rate measured by electrochemical method is greater than that determined by the weight loss method: A. an EMF is needed for pushing corrosion current through the resistance of the solution, B. Tafel behavior is interferred by concentration and resistance polarization.

C. Passivity of Co and Co-Fe Alloys

Passivity of metals is due to the formation of a protective film[19] (usually oxide) on the metals. This protective film selectively inhibits the anodic process of passing the metal ions into solution. The reason why a Co or Fe anode achieves a protective film in H_2SO_4 but not in HCl solution is discussed as follows:

Consider the case where a current is supplied from a galvanc static circuit as was used in the present investigation. The anions of the acid solution (HSO_4^-, $SO_4^=$, or Cl^-), under the potential gradient connected with the current flowing, will approach close to the metal surface with their positive part furthest from the metal. (Fig. 24)

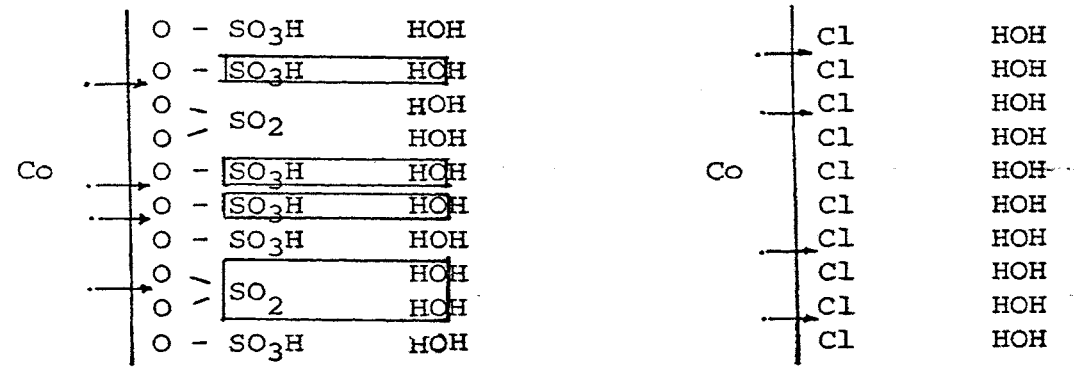

Fig. 24. Co anode in (A) H_2SO_4 solution and (B) HCl solution

If a Co or Fe electrode is subjected to anodic attack in H_2SO_4 at low current density, the metal would be expected to remain active and go into solution producing a soluble salt. The formation of metal-oxide would be impossible because of energy consideration. But as current density is fixed at a high value, the electrode potential will increase to a more noble value. Th

electrode will then provide ions sluggishly (this is especially true for the'abnormal' metals like Ni, Co, Fe...) to pass through the positive zone of the oriented HSO_4^- or $SO_4^=$ anions. However, as the desired current has to be forced through the cell, an alternative reaction must be called into play even though it may demand a larger consumption of energy. The only way to do this is for the cations to remain in the negative zone; forming oxide, and thus avoid passage through the positive zone; the rest of the oriented particle SO_2OH^+ or SO_2^{2+} is then sent into the liquid and joins $(OH)^-$ of the nearest HOH forming $SO_2(OH)_2$, and thus providin appropriate electrical transfer.

If the solution contains chloride ions and when the anode is polarized to a noble potential, the following side reaction may occur at the anode:

$$Co + 3Cl^- \longrightarrow CoCl_3 + 3e \qquad (7)$$

However, $CoCl_3$ is soluble in HOH, therefore, Co will continue to pass into solution even though the anodic current is high.

V. SUMMARY AND CONCLUSIONS

The corrosion of Co and Co-rich Co-Fe alloys in H_2SO_4 and HCl solutions proceeds according to electrochemical mechanisms. In air-free acid, the corrosion reaction is cathodically controlled and in aerated acid the reaction is probably diffusion controlled.

Co is much more corrosion resistant than Fe in deaerated acid solutions. Oxygen has a pronounced effect in increasing the corrosion of Co and Co rich Co-Fe alloys. In aerated acids, Co and Fe display about the same resistance. A sintered Co compact is inferior to solid Co as a corrosion resistant material. Generally a sintered Co compact possesses a more corrosion resistant surface than the interior. Thus the metal dissolution occurrs mostly in the interior, leaving a corrosion resistive skin.

The activation energy of dissolution of Co in 1N H_2SO_4 is 19 kcal/mole in air-free acid and 10.3 kcal/mole in oxygenated acid. Co and Co-Fe alloys show more active corrosion potentials in HCl than in H_2SO_4. However, they corrode faster in H_2SO_4 than in HCl. It is concluded that by measuring corrosion potentials alone one cannot predict the corrosion rates.

However, measurements of the corrosion potential and cathodic polarization behavior can be used to calculate the corrosion rate provided that concentration and resistance polarization is minimized to the greatest extent. It is believed that the electrochemical method may be used to accurately measure very low corrosion rates which are both difficult and tedious to perform with the conventional weight loss method.

Co and Co-Fe alloys become passive in H_2SO_4 at the anodic current densities higher than 300 ma/cm^2.

VI. APPENDIX

The appendix contains all the data necessary for plotting Figs. 6 - 21 in the corrosion studies of Co, Fe, and Co-rich Co-Fe alloys.

Tables II - VII contain the corrosion rate data for Co, Fe, and Co-Fe alloys in sulfuric and hydrochloric acids at room temperature.

Tables VIII and IX contain the data for calculating the activation energy of dissolution of Co in deaerated and oxygenat sulfuric acid.

Tables X - XIII contain the corrosion potential data of Co, Fe, and Co-Fe alloys in deaerated sulfuric and hydrochloric acid

Tables XIV - XVI contain data for the cathodic polarization potential of Co and its Fe alloys in deaerated sulfuric and hydrochloric acids.

Table XVII contains anodic polarization data for Co and Fe in deaerated 1N sulfuric and hydrochloric acids.

Table II

The Corrosion of Co-Fe Alloys in Deaerated 1N H_2SO_4

Sample: Pure Co
Surface area (dm^2): #1 0.0341 #2 0.0341

Time (hour)	Weight Loss (mg) #1	#2	Ave. Corr. Rate (mdd)
0	0.0000	0.0000	0
24	0.0040	0.0039	115
48	0.0094	0.0085	131
48.5	0.0124	0.0102	164
71.5	0.0201	0.0210	202
73	0.0180	0.0196	181
72.5	0.0165	0.0158	170

Sample: 98%Co-2%Fe
Surface area (dm^2): #1 0.0340 #2 0.0344

Time (hour)	Weight Loss (mg) #1	#2	Ave. Corr. Rate (mdd)
0	0.0000	0.0000	0
24	0.0043	0.0047	132
48	0.0088	0.0072	117
48.5	0.0107	0.0098	149
71.5	0.0210	0.0207	204
73	0.0221	0.0217	209
48.5	0.0144	0.0137	205

Sample: 96%Co-4%Fe
Surface area (dm^2): #1 0.0354 #2 0.0352

Time (hour)	Weight Loss (mg) #1	#2	Ave. Corr. Rate (mdd)
0	0.0000	0.0000	0
24	0.0049	0.0049	136
48	0.0120	0.0137	183
48.5	0.0166	0.0158	220
71.5	0.0277	0.0260	255
73	0.0299	0.0278	269
48.5	0.0201	0.0188	273

Table II

The Corrosion of Co-Fe Alloys in Deaerated 1N H_2SO_4

Sample: 92%Co-8%Fe
Surface area (dm^2): #1 0.351 #2 0.348

Time (hour)	Weight Loss (mg) #1	#2	Ave. Corr. Rate (mdd)
0	0.0000	0.0000	0
24	0.0047	0.0059	152
48	0.0121	0.0147	191
48.5	0.0166	0.0178	244
71.5	0.0298	0.0333	304
73	0.0292	0.0341	298
48.5	0.0212	0.0233	316

Sample: Pure Fe
Surface area (dm^2): #1 0.0366 #2 0.0354

Time (hour)	Weight Loss (mg) #1	#1	Ave. Corr. Rate (mdd)
0	0.0000	0.0000	0
24	0.0177	0.0174	486
48	0.0525	0.0516	723
48.5	0.0512	0.0513	705
71.5	0.0722	0.0700	663
48.5	0.0465	0.0511	671

Sample: Pure Co (sheet)
Surface area (dm^2): #1 0.043 #2 0.045

Time (hour)	Weight Loss (mg) #1	#2	Ave. Corr. Rate (mdd)
0	0.0000	0.0000	0
50.5	0.0044	0.0033	43.3
70.5	0.0061	0.0069	50.4
75	0.0101	0.0107	75.5
67	0.0131	0.0140	111
120	0.0272	0.0262	122
120	0.0343	0.0288	147

Table III

The Effect of Fe Concentration on the Corrosion Rate of Co-Fe Alloys in Deaerated 1, 2, 4N H_2SO_4 and 1N HCl

Alloys	Steady Corr. Rate (mdd)			
%Fe	1N H_2SO_4	2N H_2SO_4	4N H_2SO_4	1N HCl
0	195	315	493	105
2	205	355	470	123
4	275	393	617	188
8	330	440	705	350
100	698	1060	1520	

Table IV

The Effect of Deaerated H_2SO_4 Concentration on the Corrosion Rate of Co-Fe Alloys

Conc. of H_2SO_4	Steady Corr. Rate (mdd) Alloy in %Fe					
N	0	2	4	8	100	0 (sheet)
1	195	205	375	330	698	145
2	315	355	393	440	1060	235
4	493	470	617	705	1520	515

Table V

The Corrosion of Co-Fe Alloys in Oxygenated 1N H_2SO_4

Sample: Pure Co
Surface area (dm^2): #1 0.0343 #2 0.0345

Time (hour)	Weight Loss (mg) #1	#2	Ave. Corr. Rate (mdd)
0	0.0000	0.0000	0
24	0.0148	0.0143	423
24	0.0201	0.0185	561
24	0.0232	0.0239	683
24	0.0272	0.0307	841
48	0.0749	0.0772	1109
48	0.0808	0.0857	1210
72	0.1408	0.1231	1328
96	0.1664	0.1169	1049

Sample: 98% Co-2% Fe
Surface area (dm^2): #1 0.0345 #2 0.0350

Time (hour)	Weight Loss (mg) #1	#2	Ave. Corr. Rate (mdd)
0	0.0000	0.0000	0
28	0.0138	0.0143	351
20	0.0166	0.0176	605
24	0.0195	0.0209	598
24	0.0280	0.0294	843
48	0.0631	0.0644	922
47	0.0700	0.0718	1050
49	0.0785	0.0801	1124
72	0.1188	0.1231	1155

Sample: 96% Co-4% Fe
Surface area (dm^2): #1 0.0343 #2 0.0345

Time (hour)	Weight Loss (mg) #1	#2	Ave. Corr. Rate (mdd)
0	0.0000	0.0000	0
24	0.0112	0.0087	286
20	0.0166	0.0132	513
27	0.0259	0.0244	643
45	0.0547	0.0558	857
70	0.1140	0.1075	1126
72	0.1301	0.1240	1217
48	0.0870	0.0731	1149

Table V

The Corrosion of Co-Fe Alloys in Oxygenated 1N H_2SO_4

Sample: 92% Co-8% Fe
Surface area (dm^2): #1 0.0354 #2 0.0359

Time (hour)	Weight Loss (mg) #1	#2	Ave. Corr. Rate (mdd)
0	0.0000	0.0000	0
23	0.0114	0.0125	356
23	0.0187	0.0210	558
46.5	0.0403	0.0521	669
49	0.0551	0.0593	785
73.5	0.0800	0.1095	946
70.5	0.0958	0.1229	1043
71	0.0997	0.1256	1068

Sample: Pure Fe
Surface area (dm^2): #1 0.0366 #2 0.0365

Time (hour)	Weight Loss (mg) #1	#2	Ave. Corr. Rate (mdd)
0	0.0000	0.0000	0
21.5	0.0249	0.0217	712
24.5	0.0256	0.0228	649
25	0.0324	0.0279	792
46.5	0.0575	0.0501	760
49	0.0575	0.0533	743
47	0.0594	0.0536	789
70.5	0.0835	0.0777	740

Sample: Pure Co (sheet)
Surface area (dm^2): #1 0.0468 #2 0.0470

Time (hour)	Weight Loss (mg) #1	#2	Ave. Corr. Rate (mdd)
0	0.0000	0.0000	0
48	0.0729	0.0723	774
50.5	0.0825	0.0872	851
72.5	0.1266	0.1433	954
75	0.1396	0.1412	958
96	0.1571	0.1496	817

Table VI

The Effect of Fe Concentration on the Corrosion Rate of Co-Fe Alloys in Oxygenated 1, 2, 4N H_2SO_4 and 1N HCl

Alloys	Steady Corr. Rate (mdd)			
%Fe	1N H_2SO_4	2N H_2SO_4	4N H_2SO_4	1N HCl
0	1300	1345	1025	985
2	1228	1290	1025	1075
4	1155	1206	1040	1165
8	1065	1110	1070	1400
100	765	1025	1415	

Table VII

The Effect of Oxygenated H_2SO_4 Concentration on the Corrosion Rate of Co-Fe Alloys

Conc. of H_2SO_4	Steady Corr. Rate (mdd) Alloy in %Fe					
N	0	2	4	8	100	0 (sheet)
1	1300	1228	1155	1065	765	950
2	1345	1290	1206	1110	1025	980
4	1025	1025	1040	1070	1415	1130

Table VIII

The Effect of Temperature on the Corrosion Rate of Co in Deaerated 1N H_2SO_4

Temperature: 35°C
Surface area (dm^2): #1 0.0407 #2 0.0413

Time (hour)	Weight Loss (mg) #1	#2	Ave. Corr. Rate (mdd)
45.5	0.0117	0.0132	160
47	0.0156	0.0190	222
47.5	0.0208	0.0300	318
49	0.0303	0.0343	386
45	0.0339	0.0358	454

Temperature: 45°C
Surface area (dm): #1 0.0407 #2 0.0413

Time (hour)	Weight Loss (mg) #1	#2	Ave. Corr. Rate (mdd)
24.5	0.0229	0.0215	531
47.5	0.0846	0.0748	983
47.5	0.0816	0.0775	969
48	0.0713	0.0700	863

Temperature: 55°C
Surface area (dm^2): #1 0.0407 #2 0.0413

Time (hour)	Weight Loss (mg) #1	#2	Ave. Corr. Rate (mdd)
23	0.0682	0.0632	1672
49.5	0.1685	0.1544	1955
47	0.1277	0.1300	1605

Table IX

The Effect of Temperature on the Corrosion of Co in Deaerated and Oxygenated H_2SO_4

Tempt. °C	Max. Corr. Rate (mdd) 1N H_2SO_4 (N_2)	1N H_2SO_4 (O_2)	2N H_2SO_4 (O_2)
25	145	950	980
35	460	1380	2090
45	1020	2400	3450
55	2100	4150	5780

Table X

Corrosion Potentials of Co-Fe Alloys in Deaerated 1N H_2SO_4 at 25°C

Pure Co

Time (hr)	Potential (volt)
0	-0.0990
1	-0.1070
2	-0.1160
6	-0.1210
19	-0.1230
23	-0.1235
26	-0.1235

98% Co-2% Fe

Time (hr)	Potential (volt)
0	-0.1240
1	-0.1300
3	-0.1360
5	-0.1400
11	-0.1380
26	-0.1400
29	-0.1405

96% Co-4% Fe

Time (hr)	Potential (volt)
0	-0.1220
1	-0.1270
3	-0.1365
5	-0.1390
12	-0.1445
25	-0.1480
28	-0.1490

92% Co-8% Fe

Time (hr)	Potential (volt)
0	-0.1220
3	-0.1470
6	-0.1520
8	-0.1560
12	-0.1585
27	-0.1595
30	-0.1600

Pure Fe

Time (hr)	Potential (volt)
0	-0.2235
1.5	-0.2355
4.5	-0.2390
9.5	-0.2470
22.5	-0.2530
28.5	-0.2520
32.5	-0.2520

Pure Co (sheet)

Time (hr)	Potential (volt)
0	-0.0230
1	-0.0580
2	-0.0910
6	-0.1080
19	-0.1120
23	-0.1130
26	-0.1125

Table XI

The Effect of Temperature on the Corrosion Potential of Co in Deaerated 1N H_2SO_4

Temperature, ^oC	25	35	45
Corr. Pot., volt	-0.1125	-0.1405	-0.1660

Table XII

The Effect of H_2SO_4 Concentration on the Corrosion Potential of Co at 25^oC

H_2SO_4 Conc., N	1N	2N	4N
Corr. Pot. volt	-0.1125	-0.1065	-0.0755

Table XIII

The Effect of Fe Concentration on the Corrosion Potential of Co-Fe Alloys in Deaerated 1N H_2SO_4 and 1N HCl

Alloy (%Fe)	Corr. Pot. in HCl volt, (H_2 scale)	Corr. Pot. in H_2SO_4 volt, (H_2 scale)
0	-0.1355	-0.1235
2	-0.1665	-0.1400
4	-0.1650	-0.1490
8	-0.1870	-0.1600
100	-0.2720	-0.2520
0 (sheet)	-0.1185	-0.1125

Table XIV

Cathodic Polarization of Co-Fe Alloys in Deaerated 1N H_2SO_4 at 25°C

Curr. Dens.	Cathodic Pot., volt (H_2 scale)			
ma/cm^2	Co	2% Fe	4% Fe	8% Fe
0	-0.1235	-0.1400	-0.1490	-0.1600
0.166	-0.182	-9.177	-0.176	-0.168
0.331	-0.222	-0.215	-0.208	-0.199
0.662	-0.267	-0.263	-0.253	-0.244
1.324	-0.307	-0.307	-0.297	-0.291
2.648	-0.361	-0.354	-0.340	-0.332
5.296	-0.418	-0.401	-0.386	-0.380
10.59	-0.475	-0.452	-0.441	-0.428
21.18	-0.536	-0.508	-0.498	-0.483
43.2	-0.594	-0.575	-0.560	-0.538

Table XV

Cathodic Polarization of Co in Deaerated 1, 2, 4N H_2SO_4 and 1N HCl at 25°C

1N H_2SO_4		2N H_2SO_4		4N H_2SO_4		1N HCl	
C.D.	Pot.	C.D.	Pot.	C.D.	Pot.	C.D.	Pot.
0	-0.1125	0	-0.1065	0	-0.0755	0	-0.1185
0.116	-0.171	0.127	-0.144	0.127	-0.144	0.322	-0.257
0.232	-0.195	0.255	-0.172	0.255	-0.153	0.645	-0.299
0.464	-0.239	0.510	-0.214	0.510	-0.177	1.344	-0.341
0.928	-0.285	1.02	-0.253	1.02	-0.208	2.688	-0.388
1.856	-0.332	2.04	-0.292	2.04	-0.244	5.37	-0.430
3.712	-0.385	4.08	-0.337	4.08	-0.287	10.74	-0.464
7.424	-0.438	8.16	-0.388	8.16	-0.335	21.50	-0.504
14.85	-0.493	16.32	-0.439	16.32	-0.384	43.0	-0.561
29.70	-0.551	33.15	-0.484	33.15	-0.419		
59.40	-0.598	66.30	-0.534	66.30	-0.475		

Table XVI

Cathodic Polarization of Co in Deaerated 1N H_2SO_4 at 25°, 35°, and 45°C

Tempeature: 25°C		Temperature: 35°C		Temperature: 45°C	
C.D.	Pot.*	C.D.	Pot.*	C.D.	Pot.*
0	-0.1125	0	-0.1405	0	-0.1660
0.116	-0.171	0.167	-0.173	0.139	-0.164
0.232	-0.195	0.278	-0.182	0.278	-0.172
0.464	-0.239	0.556	-0.230	0.556	-0.188
0.928	-0.285	1.112	-0.278	1.112	-0.227
1.856	-0.332	2.224	-0.325	2.224	-0.274
3.712	-0.385	4.448	-0.374	4.448	-0.324
7.424	-0.438	8.896	-0.423	8.896	-0.380
14.85	-0.493	17.792	-0.472	17.792	-0.430
29.70	-0.551	35.584	-0.528	35.584	-0.483
59.40	-0.598				

*cathodic potential in volt (H_2 scale)

Table XVII

Anodic Polarization of Co and Fe in 1H H_2SO_4 and HCl

Co		Co		Co		Fe	
1N H_2SO_4		1N H_2SO_4*		1N HCl		1N H_2SO_4	
C.D.	Pot.	C.D.	Pot.	C.D.	Pot.	C.D.	Pot.
1.55	-0.108	0.91	-0.099	1.25	0.068	0.646	-0.240
6.45	-0.076	1.82	-0.084	5.21	0.097	1.292	-0.229
12.90	-0.065	3.64	-0.068	10.42	0.107	2.584	-0.216
25.80	-0.046	7.28	-0.045	20.84	0.117	5.168	-0.201
51.60	-0.015	15.20	-0.025	41.68	0.144	12.90	-0.177
103.2	+0.046	30.40	-0.009	83.36	0.187	25.80	-0.147
206.4	+0.141	60.80	+0.024	166.72	0.257	51.60	-0.117
322.0	+0.354	121.60	+0.091	333.44	0.400	103.20	-0.064
		243.20	+0.191	468.00	0.539	206.40	+0.057
		273.00	+0.321	521.00	0.588	412.80	+0.341
				621.00	0.642		

*no nitrogen bubbling

VII. BIBLIOGRAPHY

1. Battle Memorial Institute, "Cobalt Monograph", PP 121 (1964)

2. "Atlas of Electrochemical Equilibria", Ganthier-Villars, London, Paris and Pergamon Press, (1963)

3. Antropov, L. I., Zhur. Fiz. Khim., 26 1688 (1952)

4. Young, R. S., Corr. Tech. 4, 396, (1957)

5. Young, R. S., Corr. Tech. 6, 89, (1958)

6. Hedges, E. S., " Protective Film on Metals", PP 125, Chapman and Hall Ltd., London, (1937)

7. Hedges, E. S., J. Chem. Soc., 2881 (1926)

8. Heusler, K. E., Corr. Science, 5, 183 (1965)

9. Bond, A. P., Sc. D. Thesis, Dept. of Met. MIT (1958)

10. Hansen, M. & Anderko, P., " Binary Alloy Systems ", McGraw-Hill Book Co. Inc., New York (1958)

11. Richardson, F. D. & Jeffes, J. H. E., J. Iron Steel Inst., 160, 261 (1948)

12. Amer. Soc. Testing Mater., ASTM Std., part 2. B185-43T, 1045 (1952)

13. Whitney, W. R., J. Amer. Chem Soc., 25, 394 (1903)

14. Evans, U. R. & Hoar, T. P., Proc. Royal Soc., A137, 343 (1932)

15. Mears, R. B. & Brown, R. H., Trans. Electrochem. Soc. 74, 495 (1938)

16. Stern, M. & Geary, A. L., J. Electrochem. Soc. 104, ~~261~~ 56 (1957)

17. Evans, U. R., "An Introduction to Metallic Corrosion" Edward (Publishers) Arnold Ltd., London, PP 65 (1963)

18. LaQue, F. L. & Copson, H. R. "Corrosion Resistance of Metals and Alloys", Reinhold Publishing Corp., PP 74 (1963)

19. Evans, U. R., J. Chem. Soc., 1024 (1927)

A. Mellor, J. W., "A Comprehensive Treatise on Inorganic and Theoretical Chemistry", London, Longmans, Green & Co., Ltd, PP 451 (1924)

B. Watt, A., "Electro-Deposition", Crosby, Lockwood and Son, London, PP 351 and 517 (1889)

C. Watts, O. P., Trans. Am. Electrochem Soc., 23 99, (1913)

D. Kershner, K. K., Hoertel, F. W. and Stahl, J. C., U.S. Bureau of Mines, Report of Investigation No. 5175, Jan. 1956

VITA

The author was born on October 6, 1940 in Taiwan, China. He completed his primary and high school education in Taichung, Taiwan, China. He enrolled in Taiwan Cheng Kung University in September 1959, and received the Bachelor of Science degree in Metallurgical Engineering in June 1963.

He entered the Graduate School of the University of Missouri at Rolla in June 1966. From February 1967 to May 1968, he was a research assistant in the Graduate Center for Materials Research of the Space Science Research Center with funds provided by the Office of Naval Research and the Corrosion Research Council.